Aalto University
School of Science
Degree Programme in Engineering Physics and Mathematics

Sauli Kurki-Suonio

Continuous filaments of negatively charged cellulose nanofibrils and polyelectrolytes by interfacial complexation

Master's Thesis
Helsinki, May 30, 2016

Supervisor: Professor Olli Ikkala
Advisor: Matti Toivonen M.Sc. (Tech.)

Aalto University
School of Science
Degree Programme in Engineering Physics and Mathematics

ABSTRACT OF
MASTER'S THESIS

Author: Sauli Kurki-Suonio

Title:
Continuous filaments of negatively charged cellulose nanofibrils and polyelectrolytes by interfacial complexation

Date: May 30, 2016 **Pages:** vii + 57

Major: Engineering Physics **Code:** F3005

Supervisor: Professor Olli Ikkala

Advisor: Matti Toivonen M.Sc. (Tech.)

Cellulose nanofibrils (CNF), an important group of nanocelluloses, are promising building blocks for functional materials owing to their high mechanical strength and stiffness among other attractive properties. TEMPO-oxidation, i.e. 2,2,6,6-tetramethylpiperidine-1-oxyl oxidation, is an interesting technique for producing anionic CNF with low energy consumption. One of the most pursued goals in the field of CNF research is to produce fibers with high strength and stiffness. Such a material would have a wide range of applications, for example in textiles and fiber-reinforced composites.

Interfacial polyelectrolyte complexation is a method for producing continuous fibers by self-assembly from two oppositely charged polyelectrolyte solutions.

In this work we used interfacial complexation to prepare strong fibers from TEMPO-oxidized CNF and three different cationic moieties: a cationic surfactant and two different cationic polyelectrolytes. The fibers could be stretched prior to drying which increased their final ultimate tensile strength and stiffness in the dried state. The fibers were comparable in strength to other CNF-based fibers presented in the literature. This is the first time, to the authors knowledge, that CNF-based fibers were prepared by interfacial complexation. This work demonstrates a novel method for producing strong CNF-based fibers and further development of this method could open pathways to CNF-based fiber applications.

Keywords: nanocellulose, cellulose nanofibrils, interfacial complexation, fiber

Language: English

Aalto-yliopisto
Perustieteiden korkeakoulu
Teknillisen fysiikan ja matematiikan koulutusohjelma

DIPLOMITYÖN TIIVISTELMÄ

Tekijä: Sauli Kurki-Suonio

Työn nimi:
Negatiivisesti varautuneiden selluloosananokuitujen ja polyelektrolyyttien rajapintakompleksoinnilla valmistetut kuidut

Päiväys:	30. toukokuuta 2016	**Sivumäärä:**	vii + 57
Pääaine:	Teknillinen fysiikka	**Koodi:**	F3005
Valvoja:	Professori Olli Ikkala		
Ohjaaja:	Diplomi-insinööri Matti Toivonen		

Selluloosan nanokuidut ovat viime aikoina herättäneet suurta mielenkiintoa niin kansainvälisessä kuin suomalaisessakin tutkijayhteisössä. Selluloosan nanokuitujen lujuus ja jäykkyys yhdistettynä keveyteen ja bioyhteensopivuuteen tekee niistä lupaavan lähtöaineen tulevaisuuden materiaaleille. Viimeaikaiset edistysaskeleet selluloosan nanokuitujen valmistuksessa, kuten TEMPO-oksidointi, eli 2,2,6,6-tetrametyylipiperidiini-1-oksyyli oksidointi, vähentää nanoselluloosan tuotannossa vaadittavaa energiaa. Yksi suurimmista tavoitteista nanoselluloosan tutkimuksessa on valmistaa vahvoja ja jäykkiä kuituja, joita voitaisiin soveltaa esimerkiksi tekstiileissä ja kuituvahvisteisissa komposiittimateriaaleissa.

Tässä diplomityössä tutkittiin TEMPO-oksidoiduista selluloosananokuiduista tehtyjen kuitujen valmistusta rajapintakompleksoinnilla. Selluloosananokuituja kompleksoitiin kolmen eri kationisen aineen kanssa, joista yksi oli surfaktantti ja kaksi polyelektrolyyttejä.

Valmistettuja kuituja voitiin venyttää märkänä mikä paransi niiden lujuutta ja jäykkyyttä kuivattuina. Valmistetut kuidut olivat lujuudeltaan ja jäykkyydeltään vertailukelpoisia muualla kirjallisuudessa esitettyihin nanoselluloosapohjaisiin kuituihin. Tämä oli kirjoittajan tiedon mukaan ensimmäinen kerta, kun nanoselluloosapohjaisia kuituja valmistettiin rajapintakompleksoinnilla.

Tämä diplomityö esittelee uuden valmistusmenetelmän nanoselluloosapohjaisille kuiduille. Tämän diplomityön tuloksia voidaan hyödyntää nanoselluloosapohjaisten kuitujen jatkotutkimuksessa sekä nanoselluloosan sovelluksien kehittämisessä.

Asiasanat:	nanoselluloosa, selluloosananokuidut, rajapintakompleksointi, kuitu
Kieli:	Englanti

Acknowledgements

I would like to thank my advisor Matti Toivonen for his outstanding guidance during this project. The lengthy discussions and thorough comments were very helpful. I thank my supervisor Olli Ikkala for his valuable insights and comments for this thesis. I would also like to thank everyone in the MolMat and HYBER groups for just being so incredibly fun to work with.

Thanks to the Guild of Physics for all the fun parties, the physicist spex, student union advocacy, tutoring, songleading and sitsit. So many of my friends have been brought to my life thanks to you. A special thanks to the Aalto University Student Union songleaders of 2011 for being awesome.

I would like to thank, and I do thank, the Polytech Choir for bringing so much music in my life. Singing with you has given me many unforgettable experiences: London, Tartu, Muurla, summer sails... All the wonderful songs we've sung in our numerous concerts and quartet performances pale in comparison to the friendship and team spirit of "Parhaat Kaverit".

I thank my family for their unwavering support without which I could not have completed my studies.

I thank Susanna for her encouraging words during stressful times and her wonderful laughter during the easier times.

Helsinki, May 30, 2016

Sauli Kurki-Suonio

Contents

Abbreviations and Acronyms

AFM	Atomic force microscopy
BC	Bacterial cellulose
CMCNF	Carboxymethylated CNF
CNC	Cellulose nanocrystals
CNF	Cellulose nanofibril
CTAB	Cetyl trimethylammonium bromide
DNA	Deoxyribonucleic acid
FTIR	Fourier-transform infrared spectroscopy
HCl	Hydrochloric acid
MFC	Microfibrillated cellulose
NFC	Nanofibrillated cellulose
NaOH	Sodium hydroxide
PDADMAC	Poly(diallyldimethylammonium chloride)
PLG	Poly(α,L-glutamic acid)
PMMA	Poly(methyl methacrylate)
PSS	Poly(styrenesulfonate)
PVA	Poly(vinyl alcohol)
SEM	Scanning electron microscopy
TEM	Transmission electron microscopy
TEMPO	2,2,6,6-tetramethylpiperidine-1-oxyl
TOCN	TEMPO-oxidized cellulose nanofibrils
YM	Young's modulus

Chapter 1

Introduction

During recent years there has been significant interest in developing alternatives with low environmental footprint to materials made from non-renewable resources [1, 2]. Cellulose is one of the most attractive starting material for more sustainable materials due to several features: it is widely available, renewable, and biodegradable, and can be produced with high resource-efficiency [3].

Nanocelluloses are an interesting family of nanomaterials derived from various sources of cellulose. More specifically cellulose nanofibrils (CNF) have been recognized as a potential starting material for stiff, strong and tough films and fibers with low density combined with the possibility of transparency. Such materials have wide-spread application potential in structural and functional materials.

This work will first introduce cellulose and nanocelluloses, followed by further details of CNF-based materials, their mechanical properties and how CNF-based oriented materials have been prepared previously. Subsequently, complexation of polyelectrolytes is introduced with an emphasis on the potential of this approach to be exploited in preparation of CNF-based fibers. Finally the preparation and properties of CNF-based fibers using interfacial polyelectrolyte complexation are described.

1.1 Cellulose

Cellulose is the most abundant polymer on Earth with an annual production of about 1.5 teratons [3]. It is environmentally friendly and biocompatible [3]. Cellulose occurs naturally in plant cell walls, and by far the most commonly harvested resource for cellulose is wood.

Cellulose is produced by other organisms as well, such as tunicates and some bacteria such as the *Acetobacter xylinum* [4]. Materials derived from wood and other plant matter and rich in cellulose are among the most used materials with applications ranging from ropes, textiles and paper to timber and housing [4]. The ubiquitous use of wood in ancient times can be seen also in the English language: The word 'material' derives from the Latin word for tree trunk [4].

Wood is a biological composite material composed of cellulose, hemicellulose, lignin and some other materials, combined to a macroscopic structure. The different scales of cellulosic fibrillar structures are depicted in figure 1.1.

The cell wall structure is layered, consisting of middle lamellae, primary wall, and three secondary wall layers, named S1, S2 and S3. The primary wall is rich in hemicellulose but most of the cellulose is found in the secondary cell wall layers, especially S2 [6]. Inside the layer there are cellulose microfibrils embedded in a hemicellulose matrix [7]. The microfibrils are typically described as having a diameter of 5–50 nm [1]. The microfibrils consist of elementary fibrils bound together by hydrogen bonding with hemicellulose [3]. The elementary fibrils consist of tightly packed cellulose polymers bonded by van der Waals forces and intra- and interchain hydrogen bonding network [7]. The polymer chains in elementary fibrils are arranged in amorphous and crystalline regions, making cellulose semicrystalline [3, 7]. A schematic of the structure of the cellulose microfibril is depicted in figure 1.2.

Cellulose was identified in 1838 by Anselme Payen, who determined its chemical composition, distinguishing it from starch and its hydrolysis product dextrin [9]. The repeating unit of cellulose is depicted in figure 1.3.

Cellulose polymer is a polysaccharide which consists of a linear chain of $\beta(1\rightarrow4)$ linked D-glucose rings and has a flat ribbon-like conformation [1, 3]. The cellulose repeating unit, depicted in figure 1.3, contains two anhydroglucose rings linked together by $(1\rightarrow4)$ linkage: An oxygen atom which is covalently linked to C1 of one glucose ring and C4 of the other ring [1]. Intramolecular hydrogen bonds between hydroxyl groups and oxygen atoms result in a linear configuration of the cellulose chain [1, 10]. The intra- and intermolecular hydrogen bonds give cellulose fibrils a high axial stiffness of 110–220 GPa [1, 10, 11].

Inside the elementary fibrils the cellulose is arranged in crystalline and amorphous regions. There are multiple different crystalline

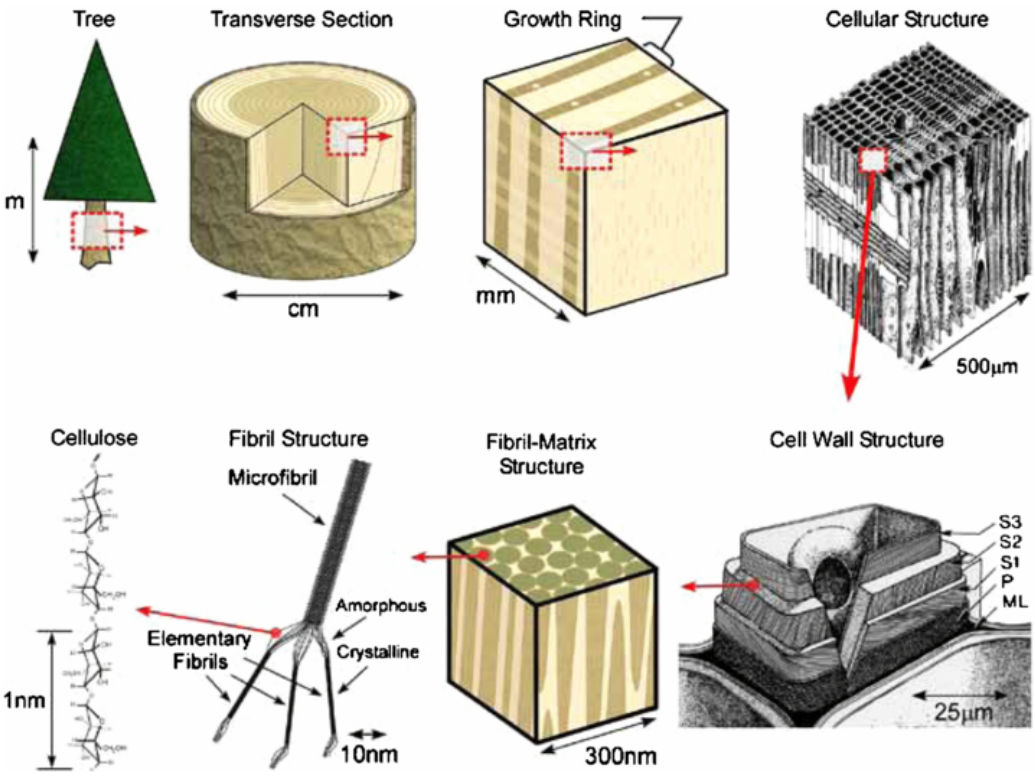

Figure 1.1: Structure of cellulose in various length scales [5].

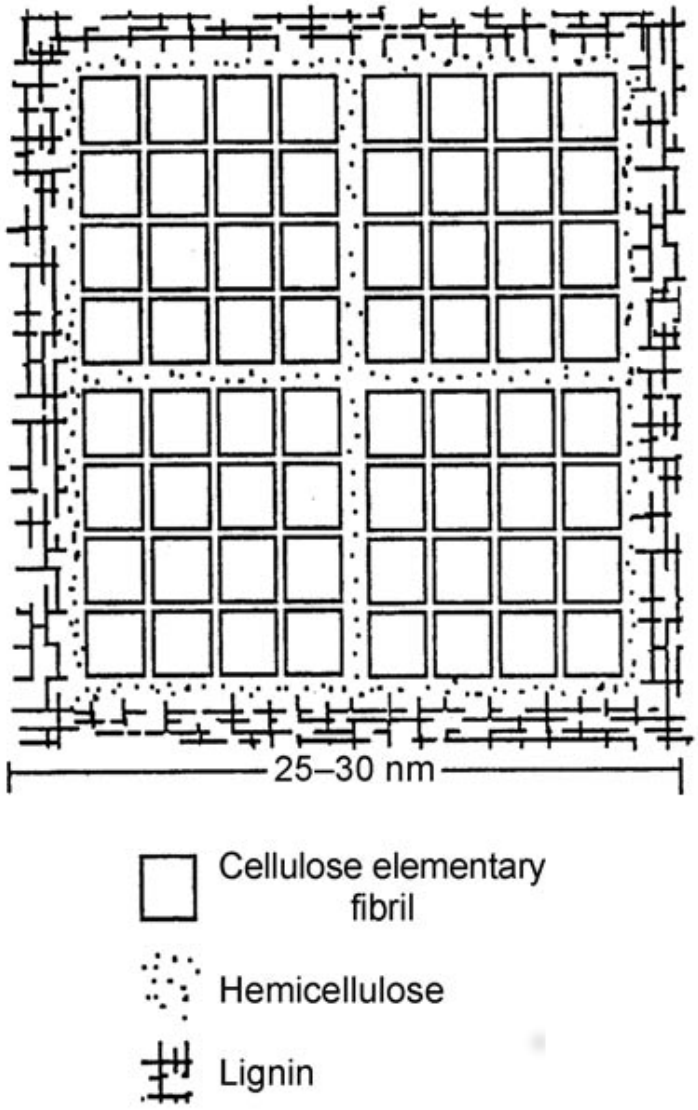

Figure 1.2: The structure of the cellulose microfibril [8].

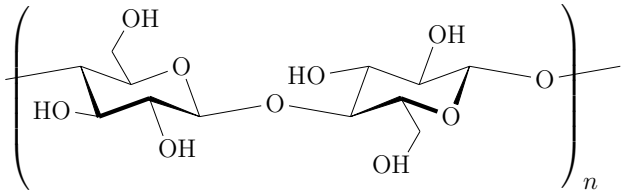

Figure 1.3: Repeating unit of cellulose molecule.

structures, or polymorphs, of cellulose denoted from cellulose I to cellulose V, but only the first polymorph, cellulose I, is produced by biosynthetic processes [1]. Cellulose I has two crystalline forms, cellulose Iα and cellulose Iβ which differ only by their hydrogen bonding network and unit cell structures [6, 12]. The ratio of cellulose Iα and cellulose Iβ produced varies between organisms. For example algae produce mostly cellulose Iα but cellulose Iβ is the dominant polymorph in trees [1].

The exact structure of elementary fibers is still up to debate [1, 13–16]. Most sources report elementary fibrils consisting of 24–36 parallel cellulose chains in a rectangular arrangement, with a lateral dimension of 3–5 nm. The elementary fibrils are formed during the biosynthesis of cellulose, as van der Waals and intermolecular hydrogen bonds between hydroxyl groups and ether groups of adjacent molecules stack multiple cellulose chains into parallel chains.

Recent methods have made it possible to cleave cellulose fibers into microfibrils and elementary fibrils and other forms of cellulose with nanometer scale features which has paved way for research towards nanocellulosic materials.

1.2 Nanocellulose

Cellulosic particles with one dimension in the nanometer range are generally referred to as nanocellulose [8, 17].

There are several distinct types of cellulose nanoparticles with distinct characteristic sizes, aspect ratios and properties. The types of nanocellulose that have gained the most attention are cellulose nanofibrils, microfibrillated cellulose (MFC), bacterial cellulose microfibrils (BC) and cellulose nanocrystals (CNC) [1].

Especially CNF's have drawn significant attention because of their good mechanical [1, 18, 19] and optical [1, 18, 20, 21] properties, potential to replace fossil fuel -based materials in some applications [18, 22],

potential for composite materials [4, 23–25] and biocompatibility [22].

The terms nanofibrillated cellulose (NFC) or microfibrillated cellulose (MFC) are also sometimes used interchangeably with CNF, but CNF is more general, as it does not refer to any type of production method. The nomenclature of cellulosic nanomaterials is not completely consistent: CNF, NFC and MFC are sometimes used interchangeably [1]. Sometimes CNF is preferred over MFC to highlight the nanosize characteristics of CNF [7]. In this text the term CNF is used.

All of these terms are not to be confused with cellulose nanocrystals (CNC), which are crystalline rodlike cellulose nanoparticles [13]. They have widely varying geometrical dimensions, with widths of 3–70 nm and lengths of 25–2000 nm depending on the source of cellulose [13]. They also have varying names, such as microcrystals, nanowhiskers and microcrystallites [13].

The sizes of the fibrillar structures of cellulose are depicted in figure 1.4. CNF's resemble cellulose microfibrils and elementary fibrils respectively in their characteristic sizes, however, the characteristic sizes of nanocelluloses depend on the production method and source of cellulose [8]. Atomic force microscopy (AFM) images of various types of nanocellulose are depicted in figure 1.5.

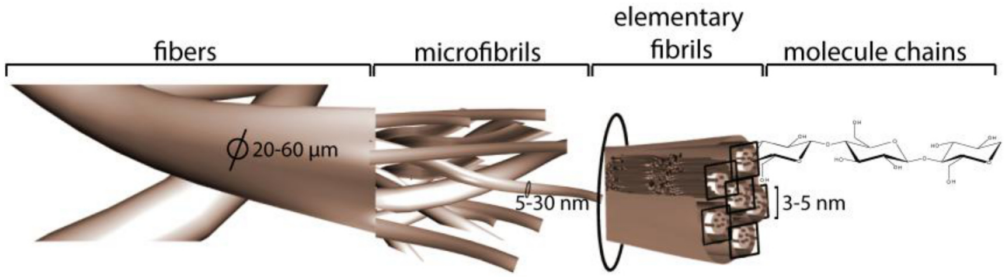

Figure 1.4: Structure of cellulose in various length scales [7].

There is usually a significant amount of hemicellulose present in plant-based CNF but its location in the fibril structure as well as its role in the properties of CNF materials is not well understood [27]. Certain bacteria produce cellulose fibers that do not contain any hemicellulose or lignin. Such fibers are structurally different from plant cellulose fibers. The bacteria secrete nanocellulose via cellulose biosynthesis as less than 100 nm wide fibril ribbons consisting

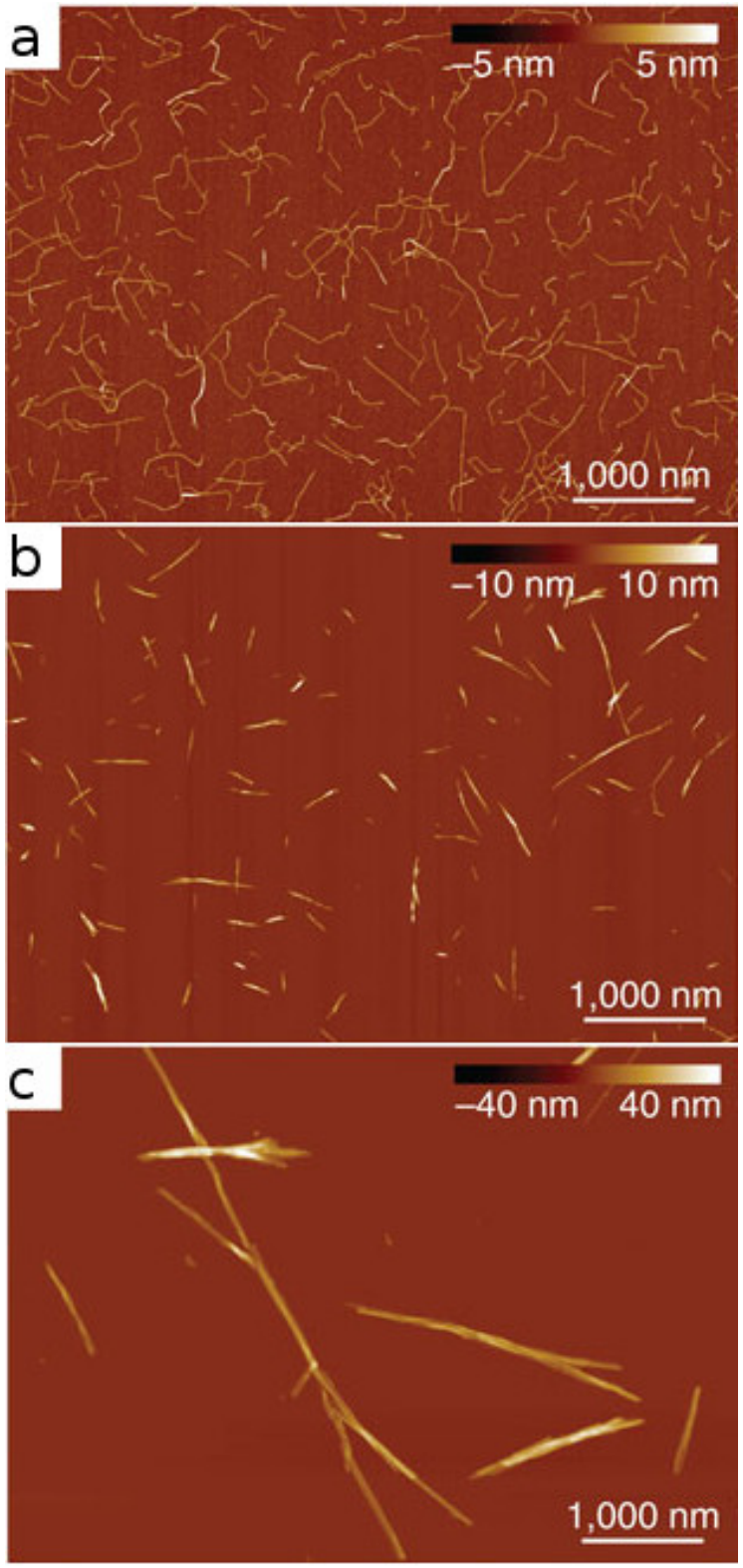

Figure 1.5: AFM images of CNF (a) and CNC (b) from wood cellulose, and CNC (c) from bacterial cellulose. Adapted from reference [26].

of nanofibrils of ca. 3 nm width [25]. The benefits of producing nanocellulose with this method are e.g. the control of the supramolecular structure and possible in situ composite formation [22]. The use of bacterial nanocellulose as reinforcement in nanocomposites has been studied recently with promising results [28–30]

Most commonly CNF is produced from wood pulp using mechanical disintegrators, ultrasonic treatment and high pressure homogenizers that cleave the larger cellulose fibers of wood into their smaller subunits, typically down to fibrillar structures approaching the elementary fibrils in diameter. Cleaving all fibrils from a suspension is not feasible but mechanical methods can be combined with filtering or centrifugation to omit the larger fibrils. Generally these disintegration methods require a lot of energy but they can be facilitated by the use of chemical or enzymatic pretreatments [1].

The use of various chemicals and enzymes has been investigated to reduce the energy requirement of mechanical production methods for nanocellulose. This usually involves introducing negative charges to the microfibril surface chemical modification. The repulsive effect of these charges then facilitates the mechanical cleaving of the fibrils.

1.2.1 2,2,6,6-tetramethylpiperidine-1-oxyl -oxidized cellulose nanofibrils

A highly efficient method of introducing charged carboxylate groups on the surface of cellulose nanofibrils was reported in 2006 [31]. This method built on the progress of studying the 2,2,6,6-tetramethylpiperidine-1-oxyl -radical, i.e. TEMPO-radical, and its catalytic properties on cellulose oxidation [32]. The TEMPO-mediated oxidation causes significant amounts of C6 hydroxyls to convert to carboxylate groups selectively on the cellulose microfibril surfaces. The electrostatic repulsion of the microfibrils combined with light mechanical disintegration results in completely individualized CNF with a high yield [33]. The oxidation reaction of cellulose is presented in figure 1.6. TEMPO-oxidized CNF (TOCN) have width of ca. 3 nm and length of several micrometers [33]. Disintegration of cellulose nanofibrils from the wood pulp fibers by purely mechanical means is energy intensive. Although TOCN fibrils require mechanical disintegration as well, TEMPO-mediated oxidation reduces this energy input requirement [33].

Similar to films made of well disintegrated unmodified CNF, self-standing TOCN films are transparent and have a high strength of

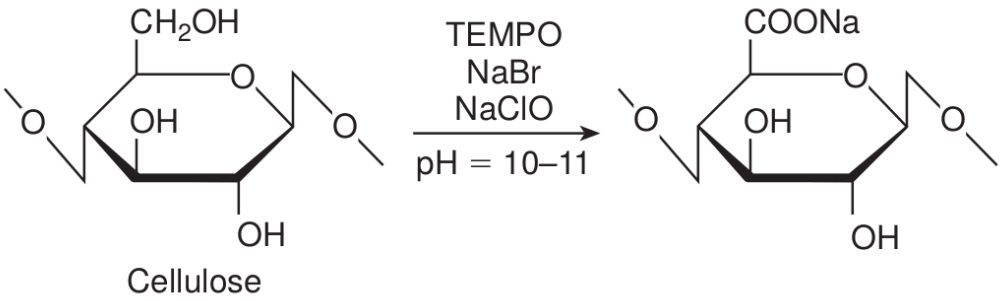

Figure 1.6: The oxidation reaction of cellulose by TEMPO-NaBr-NaClO [32].

200–300 MPa [33]. TOCN have potential applications in gas-barrier films for packaging, filters, health care materials, bioelectronics and nanocomposites [33–35].

1.2.2 Mechanical properties of nanocellulose

One of the main reasons for the interest in nanocellulose is its potential to be used in the formulation of materials with high mechanical properties in combination with low density [1, 25]. Young's modulus for individual microfibrils has varying estimates in the range of 130–220 GPa in the fiber direction and a strength of 7.5–20 GPa [1, 11, 36]. The properties of individual fibers are not fully transferred into the properties of bulk material. Neat films of CNF often have strength in the range of 80–240 MPa and a Young's modulus in the range 6–20 GPa [25]. The properties depend heavily on the source of cellulose, and neat films of BC can have strengths in the range of 87–510 MPa and Young's modulus in the range of 10–35 GPa [1]. For comparison neat films made out of wood fiber have a typical strength of 45–80 MPa and Young's modulus of 4–9 GPa [1].

The specific modulus and the specific strength of cellulose fibrils and films are presented in figure 1.7 and compared to those of common engineering materials.

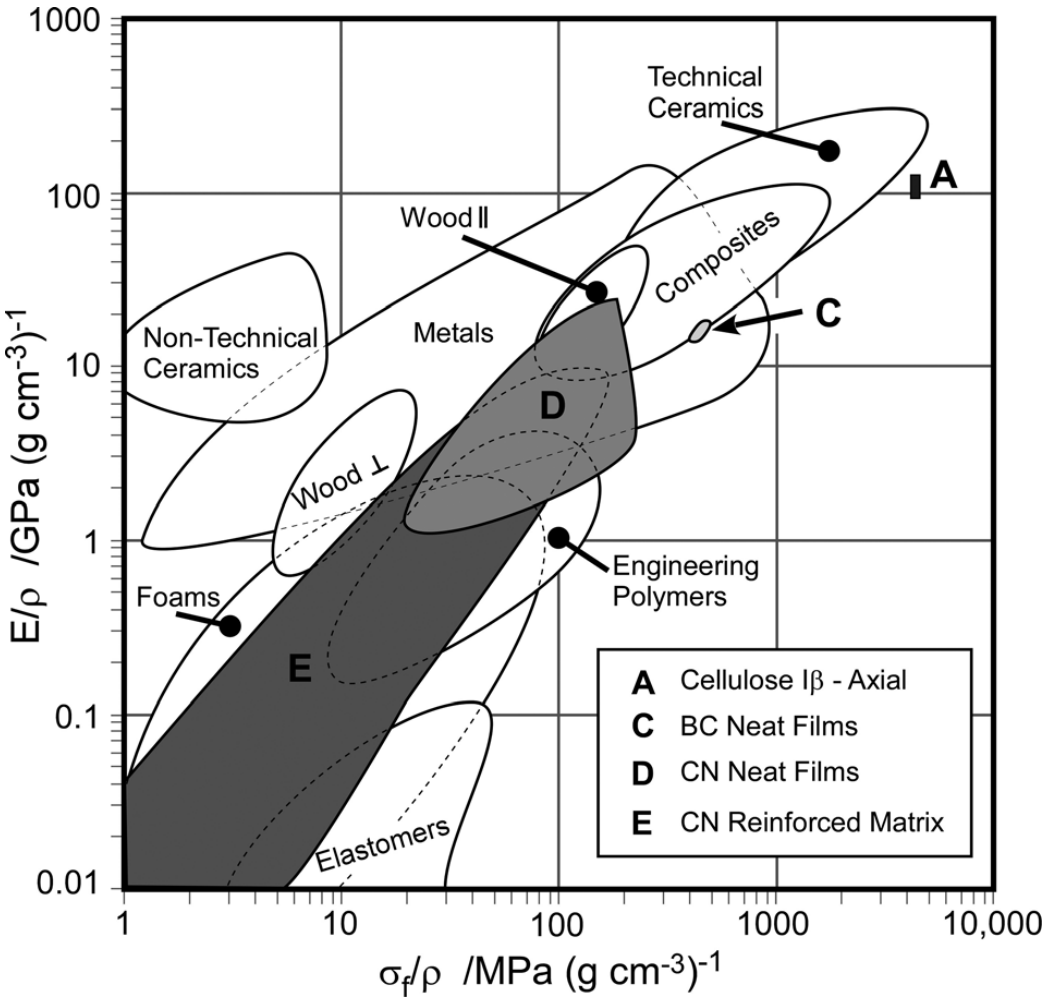

Figure 1.7: Specific modulus (E/ρ) vs. specific strength (σ_f/ρ) of various materials. The areas show values for crystalline cellulose Iβ (A), neat films of bacterial cellulose (C), neat films of CNF and CNC (D), and matrix composites reinforced with less than 30 wt. % of nanocellulose (E) [1].

1.3 Fibers and films of cellulose nanofibrils

The high axial strength of CNF has caused interest in developing nanocellulose based fibers to transfer the potential of CNF into applications.

CNF is difficult to process into fibers, requiring a tuned concentration of CNF in the source to achieve proper viscosity. The commonly

used preparation method for CNF fibers involves extruding a CNF gel or dispersion through a syringe into a coagulation bath, and subsequent drying of the fiber [35, 37, 38]. CNF can also be dry-spun by extruding on to a solid surface [39]. Another method involves a CNF dispersion flow-focusing setup with hydrodynamic alignment of the CNFs and subsequent gel-transition [40].

A way to achieve higher axial strength is to induce orientation of the nanofibrils inside the fiber. This is commonly done by stretching the fibers after spinning. Torres-Rendon et al. achieved a 28 % stretching ratio by performing the stretching slowly in aqueous environment [35], improving the tensile strength of the fiber from 118 MPa to 289 MPa. The stretching ratios commonly achieved with CNF-based fibers are low compared to synthetic fibers. There are methods of production of CNF-based fibers that result in highly oriented fibers even without stretching [38, 39, 41]. The flow-focusing setup used by Håkansson et al. induces alignment of the nanofibrils in the CNF dispersion before the gel-transition to a fiber [41].

Using CNFs as a filler material in a polymer-CNF composite fiber is a another way to achieve higher strength than CNF or the polymer alone. For example Peng et al. reached a tensile strength of 829 MPa in a polyvinyl alcohol (PVA)-CNF composite fiber [37]. Using CNF as a filler means a much lower CNF content, e.g. Peng et al. used at maximum 6 wt. % of CNF. PVA is water-soluble and biodegradable complementing the greener material aspect of CNF [37].

1.4 Polyelectrolyte complexes

Polyelectrolytes are polymers with a charged group in the repeating unit. They can be divided in polycations (positive charge) and polyanions (negative charge). Polycations most often contain ammonium-ions as the positively charged moieties. Polyanions contain most often either sulfonates, carboxylates and sometimes phosphates, as in the case of DNA. Examples of polyelectrolytes are poly(diallyldimethylammonium chloride) (PDADMAC) and poly(styrenesulfonate) (PSS), depicted in figure 1.8.

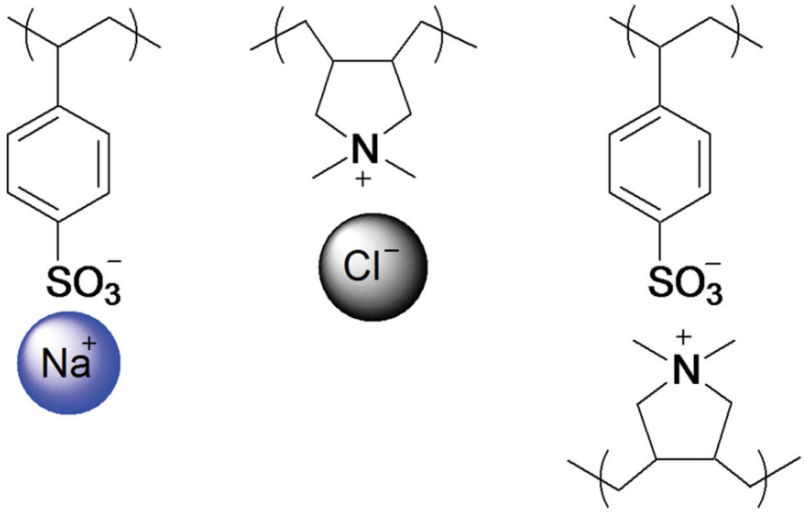

Figure 1.8: PDADMAC and PSS and ionic bonds of a polyelectrolyte complex [42].

Two oppositely charged polyelectrolytes will bind by ionic interaction and typically form an insoluble, water-rich, gel-like precipitate, sometimes called a coacervate. Ions present in the solution will also form ionic bonds with the polyelectrolytes. These ions compete with the polyelectrolyte of same charge to form ionic bonds to the polyelectrolyte of opposite charge. The bonds of polyelectrolytes and ions are depicted in figure 1.8. Interactions in polyelectrolyte complexes can be tuned by the ionic strength of the solution, much the same way as thermoplastics can be tuned by temperature [43]. The density of the crosslinks between the polyelectrolytes therefore depends on the ionic strength of the solution [43, 44]. The ionic crosslinks are reversible, resulting in an equilibrium [43, 44].

Polyelectrolyte complexes have many promising applications, such as cell growth scaffolds, drug delivery, smart actuators and sensors, self healing materials and biomechanical materials [42, 45, 46].

The complexation of oppositely charged polyelectrolytes can be used to form fibers and capsules [45]. First, the two oppositely charged polymer solutions are brought in contact forming a complex at the interface. The complex film prevents further mixing of the two polymer solutions. Then the complex film is grabbed with tweezers and drawn away from the interface. During drawing the film near the tweezers stays intact and coalesces into a fiber. Near the interface of the polymer solutions the drawing causes either new interface at the edges to be

exposed or the film to thin or break. The revealed polymers complex at this location once again completing the barrier film. Continuous drawing of the fiber causes more interfacial complexation until at least one of the polymers is exhausted.

A proposed mechanism describes the fiber formation in four stages: First the complexation of electrolytes at the interface form a viscous barrier. The drawing causes the formation of several concentrated domains of complexation. These domains then grow to nuclear fibers and finally the nuclear fibers coalesce into one thicker fiber [47]. The proposed mechanism of the fiber formation is illustrated in figure 1.9.

For a continuous fiber spinning process a sufficient supply of polyelectrolytes at the constantly revealed interface is required [45]. A high enough concentration is therefore required. Spinning rate is also a factor to be considered. Attempts to spin the fiber too fast does not give the polyelectrolytes enough time to convect and diffuse to the interface for complexation [45]. A more viscous polyelectrolyte solution might therefore require a slower spinning rate.

Ohkawa et al. were among the first to spin fiber using interfacial polyelectrolyte complexation [48]. They used an automated wet-spinning apparatus to produce an over 1000 meters long fiber with chitosan and poly(α,L-glutamic acid) (PLG). They also experimented with other combinations of polyelectrolytes reaching tensile strengths of ca. 380 MPa [48].

Stretching is the most important post-spinning method of inducing orientation in fibers. In 2003 Hachisu et al. spun fibers of poly(α,L-lysine) (PLL) and PLG using interfacial polyelectrolyte complexation [49]. The fibers could be stretched up to 200 % while immersed in water, increasing the strength by a factor of 10 reaching 147 MPa [49].

In this work we used interfacial polyelectrolyte complexation to spin fibers with anionic TOCNs and cationic polyelectrolytes and a cationic microemulsion. This is the first time, to the authors knowledge, that the interfacial polyelectrolyte complexation method is used to prepare CNF-based fibers. The wet filaments spun in this method were strong enough to be stretched by 20 %.

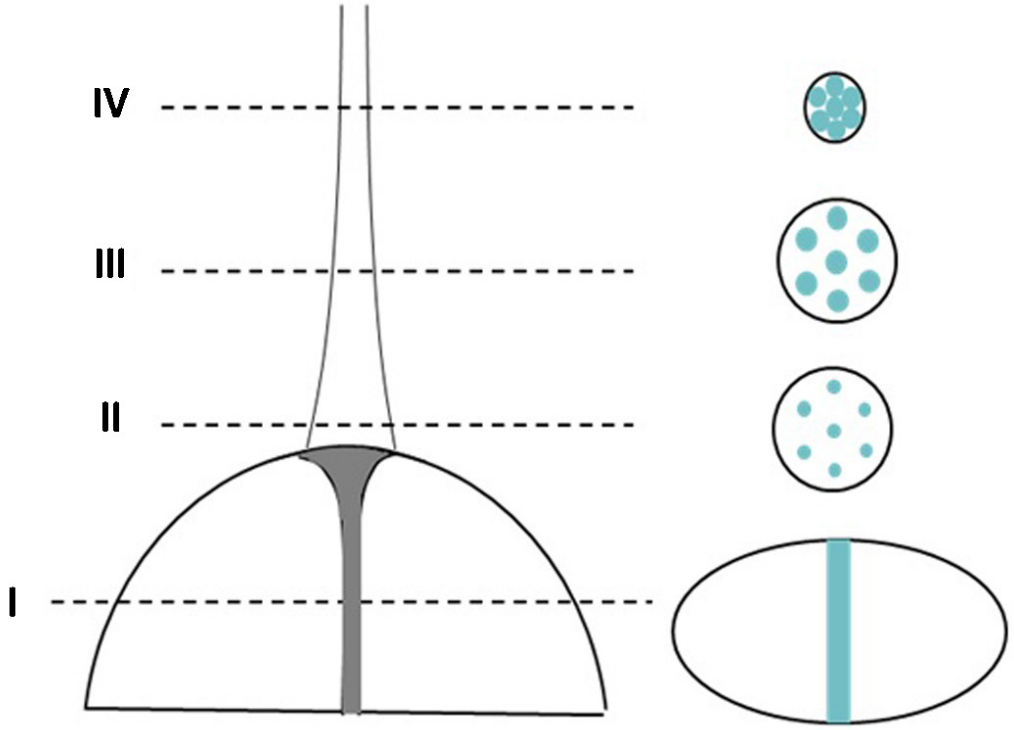

Figure 1.9: Illustration of interfacial complexation from two polyelectrolyte solution droplets. The four proposed stages of fiber formation are depicted in the cross-sectional images: (I) formation of viscous barrier, (II) formation of nucleation domains, (III) growth of nuclear fibers and (IV) coalescence of the nuclear fibers [45].

Chapter 2

Materials and methods

2.1 Materials

TEMPO-oxidized cellulose nanofibrils were prepared from birch pulp by TEMPO-oxidation followed by fluidization 3 times. It was received as 0.758 wt. % aqueous gel. 0.4 wt. % TOCN dispersion was prepared by mixing the stock TOCN gel with deionized water and mixed vigorously with a magnetic stirrer for at least 24 h. The dispersion was stored in a refrigerator to avoid microbial growth.

Three different cationic components were explored for complexation with TOCN: Two different cationic polyelectrolytes, PDADMAC and chitosan, and a microemulsion with a cationic surfactant. For brevity, they and their solutions are collectively referred to as cationic moieties or cationic solutions in the rest of the text.

PDADMAC was received from Sigma-Aldrich as a 20 % wt. solution in water and a molecular weight of 400–500 kDa. Three more PDADMAC solutions, 2 wt. %, 0.2 wt. % and 0.02 wt. %, were prepared by mixing the PDADMAC stock solution with deionized water and stirring with a magnetic stirrer for at least 1 h.

1 wt. % PDADMAC solutions with varying ionic strengths of 2.5 M, 500 mM, 100 mM, 65 mM and 20 mM were prepared by mixing the 2 wt. % PDADMAC solution with a NaCl solutions of varying molarity. One more 1 wt. % PDADMAC solution with no NaCl was prepared by mixing the 2 wt. % solution with deionized water.

Medium viscosity chitosan had molecular weight of 300–500 kDa and was received from Sigma-Aldrich as dry powder and dissolved in 100 mM (0.36 wt. %) hydrochloric acid (HCl) as 2 wt. % solution. The pH was then adjusted to 5.8 by dropwise dilution with 30 mM

(0.12 wt. %) sodium hydroxide (NaOH) during vigorous mixing, until proportion of chitosan was 1 wt. %. Two more 1 wt. % chitosan solutions were prepared by adjusting the pH of 2 wt. % chitosan solution with 32 mM (13 wt. %) and 35 mM (14 wt. %) NaOH solutions respectively to reach final pHs of 6.0 and 6.2 respectively.

The cationic surfactant we used for the microemulsion was cetyl trimethylammonium bromide (CTAB). It was received from Sigma-Aldrich as a powder. A stock solution of CTAB was prepared by mixing CTAB:1-butanol:water in 15:6:79 weight ratios respectively, and then diluting with deionized water to 1:10 weight ratio to achieve an aqueous microemulsion of CTAB and 1-butanol with a final concentration of 1.5 wt. % CTAB. The above mentioned mixing ratio was selected because it produced a low viscosity and stable microemulsion at ambient conditions.

2.2 Fiber spinning and stretching

Fibers could be spun manually or by a more controlled method of spinning by linear stage. The linear stage is described in detail in section 2.8.

2.2.1 Preliminary experiments on fiber spinning

In the preliminary tests the fibers were spun manually. A 5–30 mg droplet of TOCN dispersion was placed on a polystyrene Petri dish. A droplet 5–30 mg of cationic solution was placed near the first droplet. The droplets were brought into contact with the tip of tweezers while carefully avoiding mixing. In appropriate conditions a gel-like interface formed between the droplets instantaneously preventing further mixing. The interface was visible to the naked eye. The interface was grabbed by tweezers and by pulled upwards forming a continuous filament. The filament formation ended by rupture of the forming gel filament, usually from the tweezers, or by exhaustion of TOCN or cationic component.

2.2.2 Spinning with the linear stage

Spinning with the linear stage required small wells to be filled with TOCN and the cationic component, and the interface was pulled by a controlled linear stage with a constant velocity. Photos of the linear

stage spinning setup are presented in figure 2.1. Two types of wells were used: glass vials were used for TOCN-CTAB samples and drilled holes in PMMA blocks which were coated with a superhydrophobic agent were used for TOCN-polycation samples.

In the latter case, several blocks of 2 cm×2 cm×2 cm were cut from PMMA, shown in figure 2.1. Holes were drilled in the blocks with varying diameters of 2–15 mm and a depth of roughly 10 mm. The inside wall of the hole was cleaned with ethanol and deionized water and then coated with a Glaco superhydrophobic coating spray for car mirrors (www.glaco.jp). The coating deteriorated quickly, usually in a single use. The coating was then removed by ethanol and abrading with a paper towel and a cotton swab and deionized water. After cleaning and drying the well could be re-coated with the spray.

A well was placed on the linear stage. Few drops of TOCN dispersion were dropped in the hydrophobic well and then few drops of cationic solution on top of it. The interface was grabbed by inverted tweezers which were then attached to a stand. Photos of the linear stage spinning setup are presented in figure 2.1. The linear stage was lowered with a constant velocity, causing continuous interfacial complexation to form a wet filament. A series of photos of the spinning with linear stage is presented in figure 2.2. After the stage stopped the filament was cut from the bottom with scissors. After that the filament could be attached for drying or stretching with the linear stage.

2.2.3 Stretching of the wet filaments

The stretching was preformed with the linear stage. The top of the filament was attached to a wooden clothespin fixed on a stand. The bottom of the filament was then attached to another similar clothespin attached to a linear stage. The length of the filament could be measured with a measuring tape. The filament was then stretched with a constant chosen speed to a chosen length. After that the fiber could be left hanging on the clothespins to dry or lifted elsewhere to dry. Dry fibers were stored in polystyrene boxes.

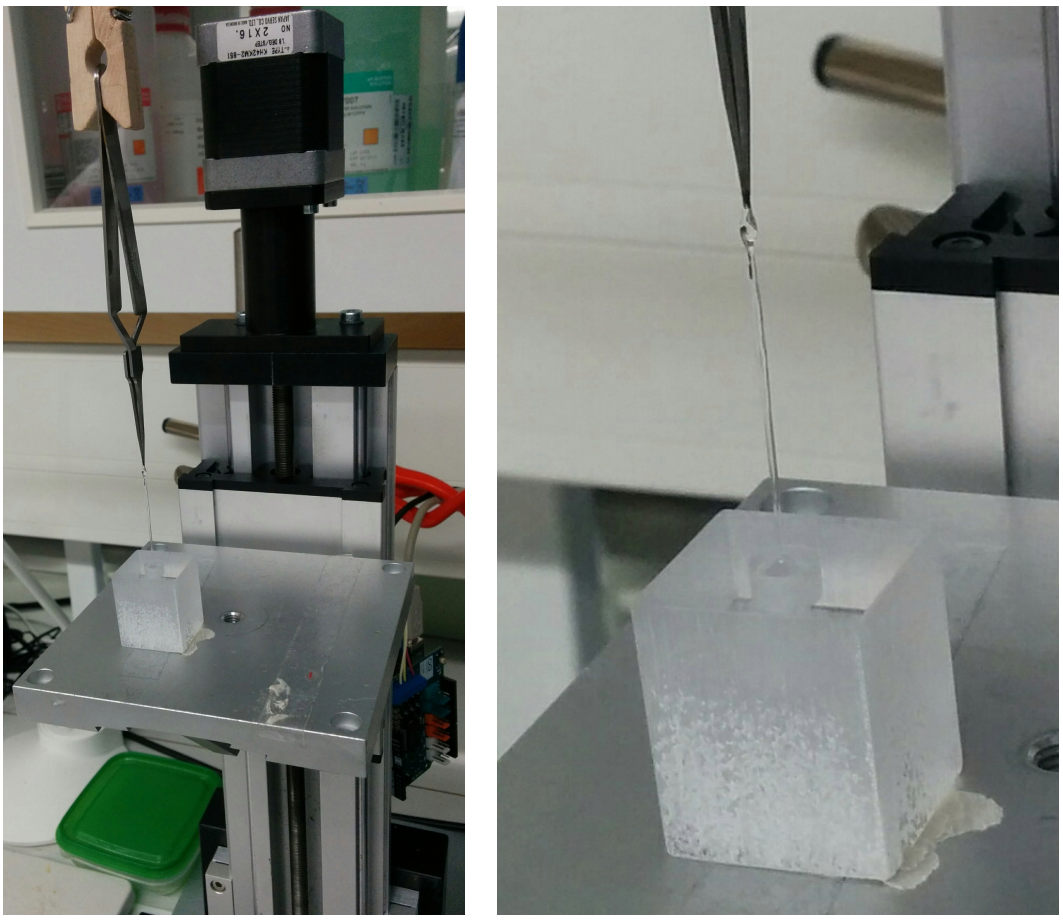

(a) The linear stage, inverted tweezers and PMMA well set up for spinning.

(b) The interfacial complex grabbed with the tweezers.

Figure 2.1: The linear stage, inverted tweezers and PMMA well set up for spinning.

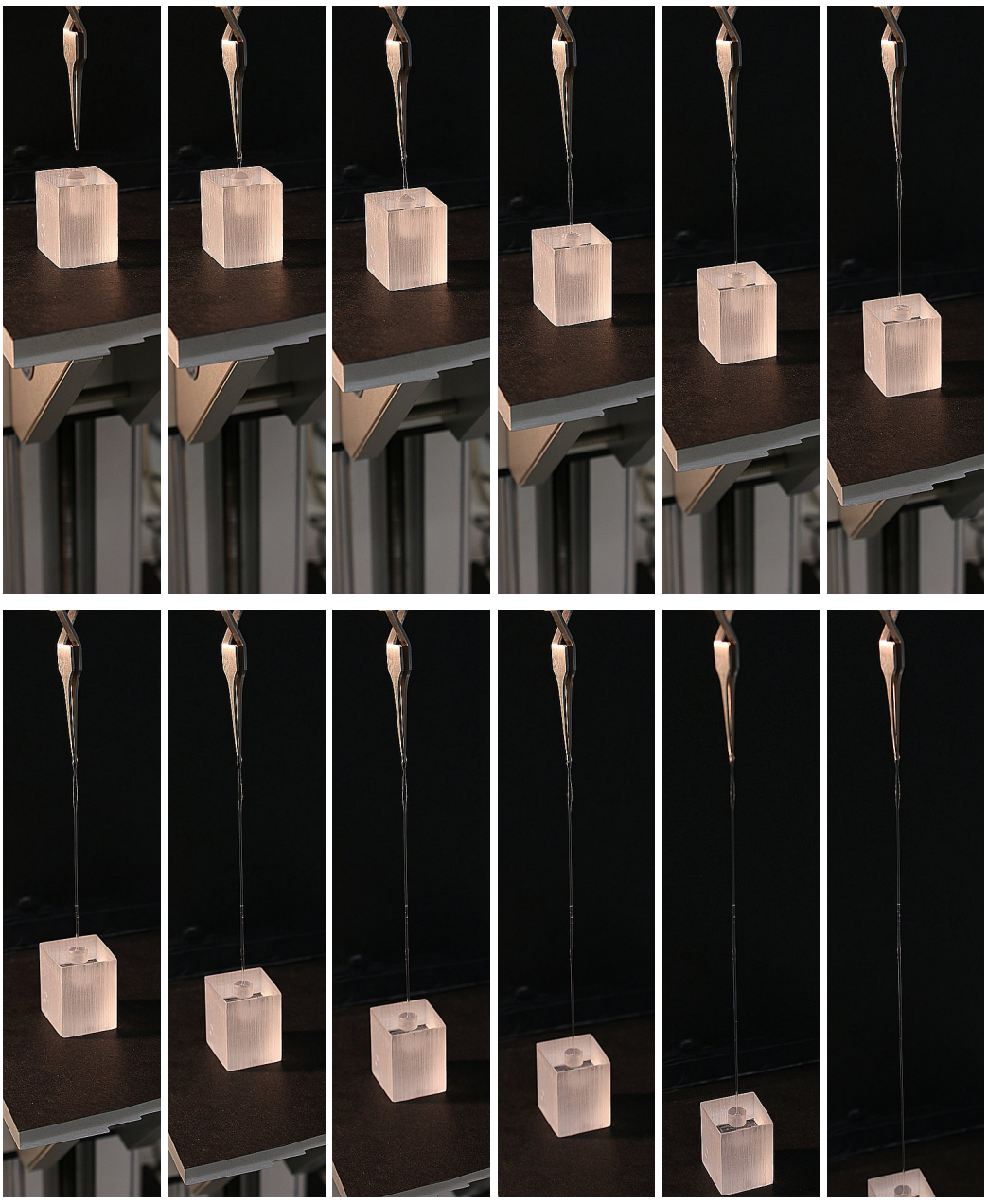

Figure 2.2: A series of photos of the spinning of a TOCN-polyelectrolyte filament. Black cardboard was placed in the background for increased visibility. An edge sharpening algorithm was used to further increase filament visibility.

2.3 Cellulose nanofibril-surfactant fiber preparation for tensile characterization

Approximately 3 ml of TOCN dispersion was put in a 12 ml glass vial with an inner diameter of 24 mm. 3 ml of CTAB solution was carefully placed on top of TOCN dispersion with plastic Pasteur pipette. The TOCN-CTAB interface was grabbed with inverted tweezers and a ca. 15 cm wet filament was spun with a constant speed of 180 mm/min. Three filaments were spun. One wet filament was left untreated and dried. One wet filament was stretched with the linear stage using constant stretching speed of 4 %/min and then dried. One wet filament was washed from excess CTAB, essentially leaving a TOCN fiber. Washed filament was allowed to dry after spinning, then washed by soaking in 100 mM HCl for 15 min, then 50 % ethanol for 15 min, then with deionized water for 15 min and then dried. Samples for mechanical testing were prepared as explained in section 2.13.

2.4 Cellulose nanofibril-polyelectrolyte fiber spinning feasibility

A fiber spinning was attempted manually without the linear stage with each combination of chosen TOCN and polyelectrolyte concentrations as described in section 2.2.1. If at least 10 cm fiber could be spun, then the concentrations were regarded as feasible for spinning.

The effect of ionic strength of PDADMAC solution and the pH of chitosan solution on the spinning feasibility was tested.

2.5 Effect of well diameter on the diameter of dry fibers

TOCN-chitosan fibers were spun with the linear stage using PMMA well with diameters varying between 2–15 mm. The fibers were dried and their diameters were measured with an optical microscope.

2.6 Cellulose nanofibril-polyelectrolyte wet filament stretching

Various filaments were spun with the linear stage using 0.4 wt. % TOCN dispersion and 2 wt. % PDADMAC or 1 wt. % chitosan solutions. The wet filaments were then stretched with a constant stretching speed of 0.4 wt. % until fracture. The initial and final distance between the fiber grips were measured with a measuring tape. A photo of the stretching setup is presented in figure 2.3

The NaCl concentration of PDADMAC solution was varied from 0 to 200 mM to test the effect of ionic strength of PDADMAC to the stretchability of the resulting wet filament. Spinning with higher NaCl concentrations was unsuccessful.

The pH of chitosan solution was varied between 5.8 and 6.2 to test the effect of protonation of chitosan to the stretchability of the resulting wet filament. The pH of chitosan solutions was measured with JENCO 6230N electronic pH meter.

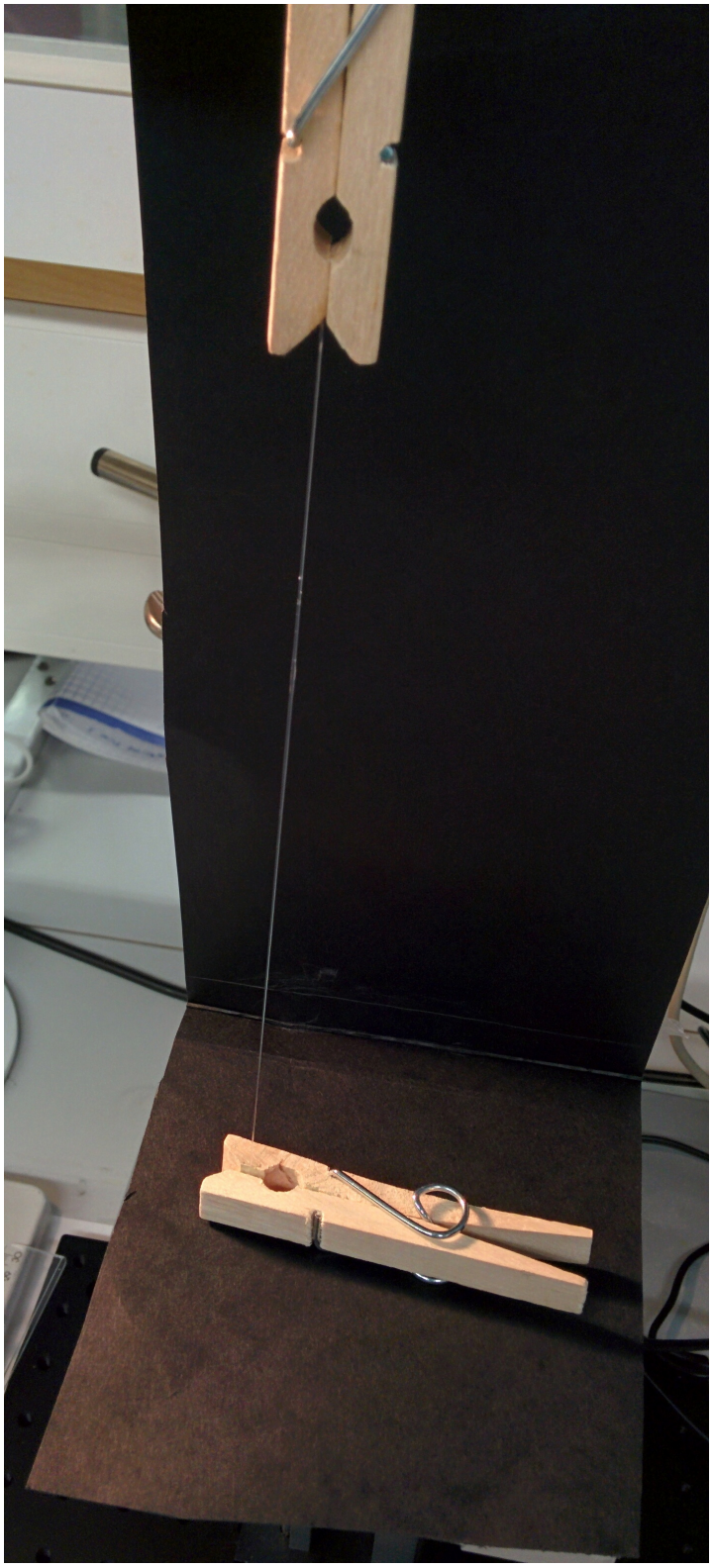

Figure 2.3: The stretching setup for wet filaments. The black cardboard background was added for increased visibility of the wet filament.

2.7 Cellulose nanofibril-polyelectrolyte fibers for tensile characterization

Approximately 0.5 ml of 0.4 wt. % TOCN dispersion was put in a 6 mm diameter PMMA well using a plastic pipette. Approximately 0.5 ml of 1 wt. % pH 5.8 chitosan solution was carefully placed on top of TOCN dispersion with a plastic pipette avoiding mixing. The complexation interface was grabbed with tweezers which were then attached to the linear stage. Two 150 mm long wet filaments were spun at a constant rate of 180 mm/min. The other wet filament was stretched to 20 % at a rate of 4 %/min while, and then left to dry. The other wet filament was untreated and simply left to dry. The procedure was repeated with 1 wt. % 0 NaCl PDADMAC solution used in the place of chitosan.

2.8 Linear stage

A linear stage was constructed using a bipolar stepping motor (type KH42KM2-851, Japan Servo Co. Ltd.) and an aluminium frame was assembled. The motor was controlled with an Arduino One open-source electronics prototyping platform and an Arduino Shield motor driving unit. The motor speed and amount of travel distance was controlled by a computer with Arduino IDE script ("sketch" in Arduino parlance) via a USB cable. The stage was used to spin and stretch filaments by vertical movement with controlled speed and distance. A photo of the Arduino platforms are presented in figure 2.4.

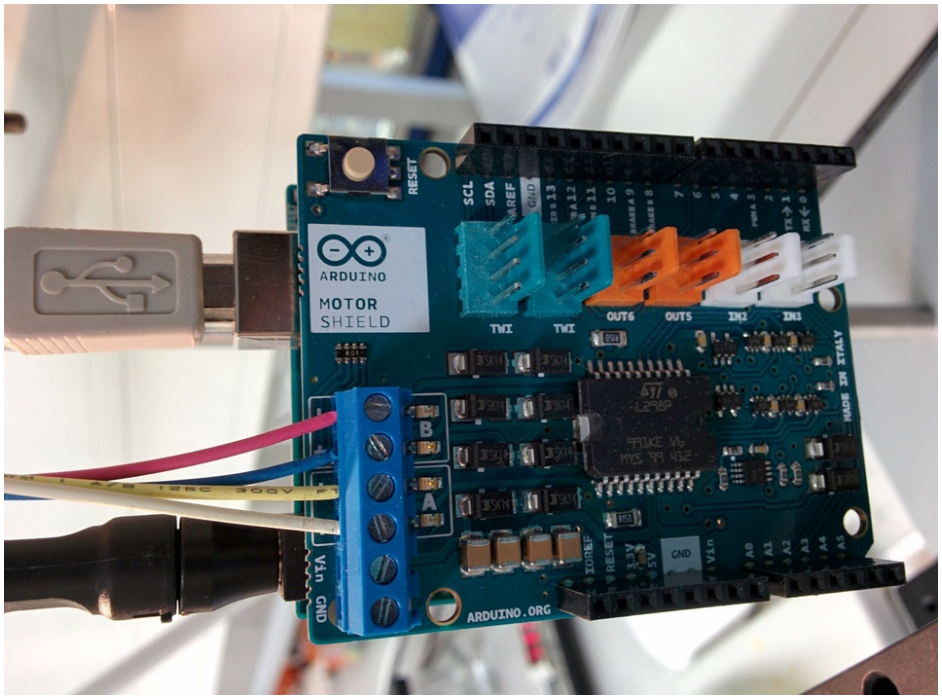

Figure 2.4: The Arduino Shield motor driving unit inserted on top of the Arduino One electronics prototyping platform.

2.9 Scanning electron microscopy

Scanning electron microscopy (SEM) is microscopy technique which uses electrons instead of light in order to achieve higher resolution and magnification. Optical microscopes are limited by the Rayleigh criterion, which describes the minimum distance between objects so that the objects are distinguishable, or the spatial resolution.

$$\Delta l = 1.220 \frac{f\lambda}{D} \tag{2.1}$$

where l is the spatial resolution, f is the focal distance, λ is the wavelength of the light and D is the diameter of the lens aperture. The factor 1.220 is determined by the position of the first dark circular ring surrounding the central Airy disk of the diffraction pattern. Electrons have a much shorter de Broglie wavelength than visible light, which makes it possible to have a much better spatial resolution with SEM.

SEM produces images by scanning a sample with beam of high energy electrons, typically 1–30 keV. Backscattered electrons, secondary

electrons or X-rays produced in the sample are then detected.

SEM has a large depth of field, which makes it useful for imaging samples with complex topography, even when the resolution of an optical microscope would be sufficient. It can also be used to detect the composition of a sample by the energy spectrum of emitted X-rays.

Zeiss Sigma VP field emission scanning electron microscope was used to image the cross-sections of the TOCN-polyelectrolyte fibers post-fracture. A ca. 10 nm metallic coating was sputtered on the samples using Emitech K100X sputter and a Au/Pd target.

2.10 Fourier transform infrared spectroscopy

Fourier transform infrared spectroscopy (FTIR) was performed on the samples with Nicolet Magna 750 FTIR spectrometer. The total attenuated reflectance of the sample fibers was measured averaging from 64 scans of the range 4000–525 cm^{-1} with a resolution of ca. 0.5 cm^{-1}.)

2.11 Determining the cross-sectional area of the fiber

The cross-sectional area, which is used to calculate stress, scales to the second power of the diameter. The error the diameter therefore strongly affects the accuracy of the strength of the fiber. For this reason an accurate measurement of the diameter was necessary. The average cross-section of the samples could then be determined by one of the following methods:

Weighing the fiber and then calculating the cross-section by approximating the density of the fibers as the density of cellulose, 1.46 $\mathrm{g/mm}^3$. The average cross-section is then obtained from

$$A = \frac{m}{l\rho}, \tag{2.2}$$

where m is the mass, l is the length and ρ is the density of the sample. This method is insensitive to the variation of the diameter along the fiber and only measures the average. It also ignores pores and hollowness of fibers, and measures the average cross-sectional area of the fiber regardless of the shape of the cross-section.

Another method is to approximate the fiber as cylindrical in shape and measure the diameter of the fiber by optical microscopy. The cross-section is then obtained from

$$A = \pi r^2, \tag{2.3}$$

where r is the radius of the sample.

One more method is to image the cross-section of a fiber after breaking with a SEM and use image processing software to measure the surface area of the cross-section, assuming the fiber is parallel to the electron beam.

A commonly used method to measure the diameter is the micrometer screw. Measuring the diameter with a micrometer screw was tested but discarded due to inaccuracy compared to SEM and optical microscopy. We observed that the diameters measured with micrometer screw were often tens of percents smaller than what was measured by optical microscopy and SEM, which were considered reliable methods. Using micrometer screw would have grossly exaggerated mechanical strength of the fibers due to error of the cross-sectional area scaling to the second power in the error of the diameter.

2.12 Optical microscopy

Optical microscopy was performed with Leica 4500D and Leica application suite. The diameter of the fiber was measured from at least 2 different points from across at least 2 images using the parallel line distance tool. The measurements were averaged for each sample. The standard deviations of diameter measurements over one sample were less than 10 %. The validity of the diameter measurements were verified with post fracture SEM images from selected samples.

2.13 Tensile characterization

Fibers were cut into ca. 20 mm long samples avoiding visible defects. Two pieces of sandpaper were glued to both ends of the samples to prevent slipping during tensile testing. The gauge length of the tensile tester was set to 10 mm and thus the sandpapers were glued 10 mm apart. The samples were placed in a humidity box with a controlled 50 % relative humidity at 22–23 °C for approximately 48 hours before

testing. The tensile testing was also preformed inside the humidity box but operating the tester caused fluctuations in the relative humidity.

All tensile characterization was preformed with Kammrath & Weiss tensile tester using 100 N load cell. The samples were attached to the tensile tester at 10 mm gauge length and elongated with a constant rate of 8.35 µm/s while measuring the tensile force of the fiber with 20 ms intervals until the sample fractured. A schematic of the tensile testing setup is presented in figure 2.5. The data from the microtester was imported to MATLAB r2015b for processing. Most of the figures were created using the matplotlib library (version 1.4.2) for Python (version 3.4.3).

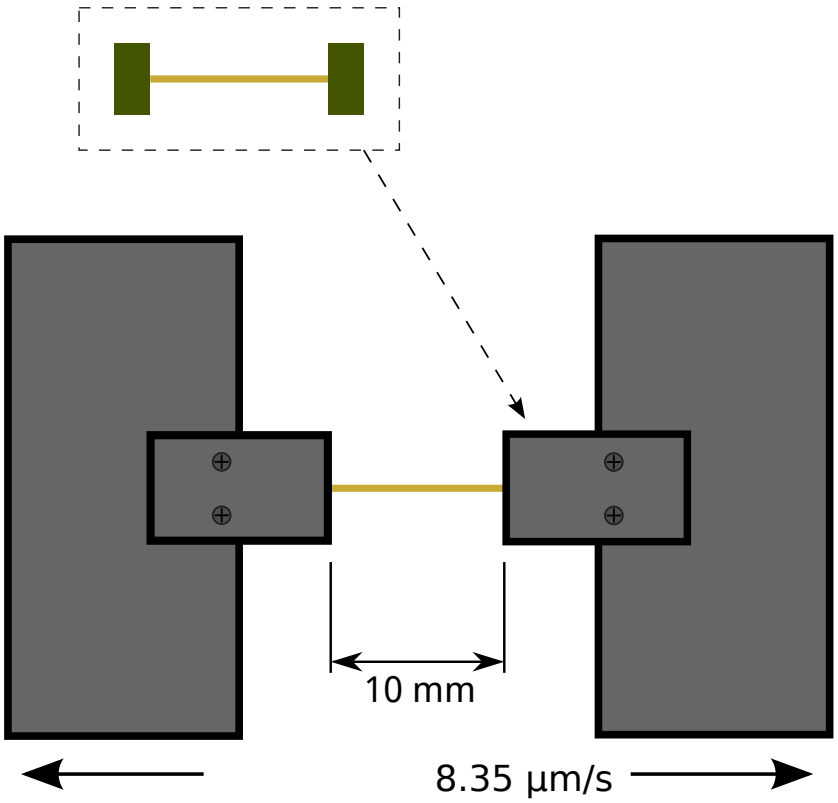

Figure 2.5: A schematic of the tensile testing setup.

The force data was smoothed to reduce noise introduced by the load cell. The force was divided by the cross-section to acquire (engineering) tensile stress. The elongation of the sample was divided by the gauge length to acquire strain.

Often samples were slightly longer than the gauge length of the tensile tester when the testing was started. This resulted in a 0–

400 µm elongation region with little to no increase in stress, also known as a toe. The toe was removed from the data with a linear inter/extrapolation from the elastic region of the stress-strain curve. The toe removal was not forced on data for which it did not seem to apply, e.g. in cases where the Young's modulus reaches its maximum very early in the measurement.

The stress-strain curve of each sample was plotted. The curves with highest and lowest ultimate tensile strength were omitted, as well as outlier curves.

Chapter 3

Results and discussion

3.1 Cellulose nanofibril-surfactant fibers

In the first part of this work we studied the spinning of the gel-like TOCN-CTAB interfacial complex that could be dried to a fiber.

We successfully spun fibers by interfacial complexation of a TOCN dispersion and a CTAB solution. The spontaneous formation of gel-like TOCN-CTAB interface demonstrates the ability of cationic surfactant to adsorb to the anionic TOCN fibrils. The fibrils possibly adhere to each other via the CTAB molecules hydrophobic ends that stick together by hydrophobic interactions.

The spinning relied on gel-like surface formation at the interface of the TOCN and CTAB solutions. At the interface the anionic TOCN fibrils and the cationic CTAB molecules interact strongly and the CTAB molecules adsorb to the TOCN surface. An interface is formed which prevents TOCN and CTAB from further aggregating. Grabbing the surface with tweezers and pulling it increases the surface area of the interface which causes more CTAB molecules to adsorb to the newly revealed TOCN fibrils. This kind of interfacial complexation could be continued until one of the components is exhausted. A schematic of the filament formation by interfacial complexation is presented in figure 3.1.

It was possible to continuously spin fiber by this interfacial complexation because the wet filament is strong enough to support its own weight up to a length of meter. The low viscosity of the TOCN dispersion and CTAB solution was interpreted to be crucial to feed new TOCN fibrils and CTAB moieties to the continuously forming interface. Because of the high strength of the wet filament

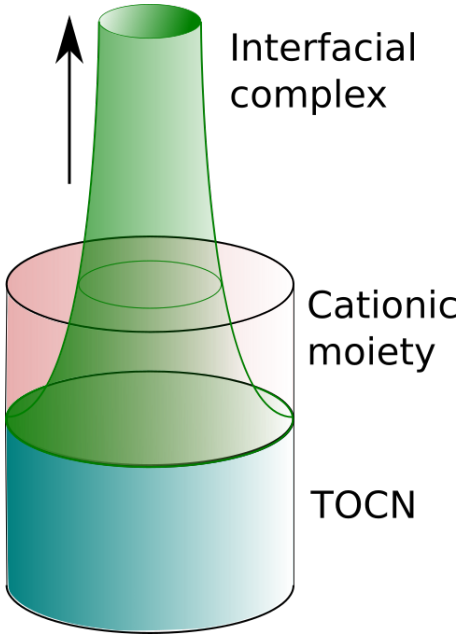

Figure 3.1: A schematic of the interfacial complexation.

we believe that new material for complexation is revealed mostly at the walls of the container. This is supported by the observation that poor hydrophobicity of the container walls often resulted in filament rupture during spinning: If the filament is adsorbed to the container wall during spinning no new material can be exposed for further complexation and attempts of spinning result in stretching the filament until it breaks.

We studied the effects of CTAB concentration to the formation of the interface and mechanically characterized fibers from concentrations we believed to be optimal. We also studied the effects of stretching and the removal of CTAB to the strength of the fiber.

3.1.1 Conditions for drawing fiber from interface

Successful manual fiber spinning was achieved with a wide range of CTAB solution concentration. A range of 0.4–17 wt. % of CTAB was found to be feasible. The concentration of the TOCN dispersion was kept constant at 0.2 wt. %. A concentration of 0.4 wt. % for CTAB and 0.2 wt. % for TOCN were selected for further work.

3.1.2 Fiber stretching

We successfully stretched wet TOCN-CTAB filaments using a linear stage with typical stretch ratios of 20–30 %.

The reached stretch ratios are comparable to wet stretched CNF-based fibers reported in the literature [35], but falls far from the best synthetic fibers [50, 51].

Significant variability between stretchability of individual wet TOCN-CTAB filaments was observed. While some filaments could be stretched more than 30% others fractured before 20%. The reason for this variability is not clear. One possible explanation could be the adsorption of TOCN or CTAB or the complex to the walls of the glass vial. Sometimes during spinning this could be observed visibly and it resulted in wet filaments with poor strength. Absorption of the components or the complex on the glass walls even to a small degree could lead to inhomogeneous stress development during spinning, generating defects.

Another possible explanation is that to stretch the wet filament it had to be stretched quickly after it was spun. This meant that it was already drying during stretching. This may place limits to stretching in ambient conditions.

3.1.3 Washing and Fourier transform infrared spectra

One TOCN-CTAB fiber was treated with 100 mM HCl to remove the CTAB from the fiber. The acid protonates the carboxyl groups making them neutral in charge. This inhibits the ionic interactions between CTAB molecules and TOCN fibrils. The CTAB molecules were rinsed away with 50% ethanol solution and then with washed with water.

The FTIR spectra of pure TOCN, pure CTAB and washed and unwashed TOCN-CTAB fibers are presented in figure 3.2. The peaks in the regions 2500–3000 cm^{-1} and around 1400 cm^{-1} of the TOCN-CTAB fiber before washing are visually similar to the peaks of CTAB in the same regions. The peaks are missing from the FTIR spectrum of TOCN-CTAB fiber after washing. This supports the claim that acid washing removes CTAB molecules from the fiber.

When comparing the peaks in the 1500–1800 cm^{-1} of TOCN and TOCN-CTAB fiber after washing one can observe that the largest peak is slightly shifted towards higher wavenumbers. This suggests that the carboxylic acids in TOCN fibrils are not deprotonated, unlike before the

washing. This might reduce the comparability of the results between the washed TOCN-CTAB fibers and other fibers presented in this work.

3.1.4 Tensile properties

The comparison between stress-strain curves for TOCN-CTAB fibers is presented in figure 3.3. The untreated fiber has the highest ultimate tensile strain and the lowest ultimate tensile strength. The washed fiber has the lowest ultimate tensile strain and highest ultimate tensile strength. The stretched fiber is between the two. Relative humidity during testing was 39–46 % at 23 °C.

The stretching results in increased yield strength and ultimate tensile strength while sacrificing some ultimate tensile strain as commonly observed in fibers and nanocomposite films [35, 52]. The washed fiber expresses similar but much more pronounced effects. Removing the CTAB from the fiber reduces the mass and also diameter of the fiber and CTAB probably does not increase the strength of the dry fiber very much. The reduced mass and diameter of the fiber by CTAB removal is not the likely explanation to the increased strength of the fiber. If the increase in strength was due to smaller diameter in the fiber because the CTAB was removed, that would still not explain the reduced ultimate tensile strain. The hydrophobic moieties of CTAB are likely to play a role in the strength of an wet filament, but when the fiber is dried the role hydrophobic interactions are reduced and the alkyl chains of CTAB only interact by Van der Waals forces.

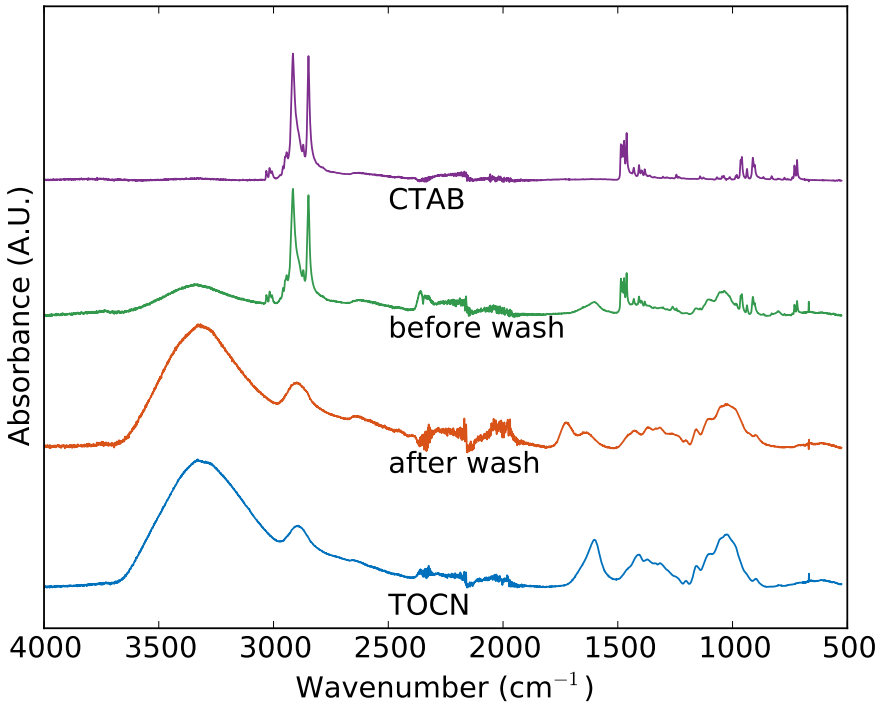

(a)

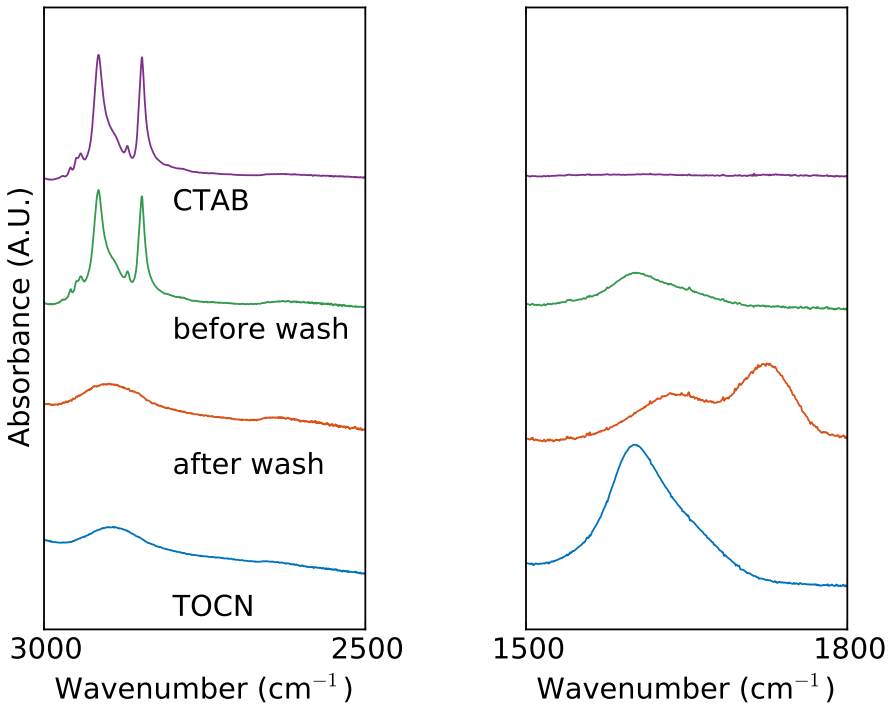

(b)

Figure 3.2: FTIR spectra of CTAB, TOCN and TOCN-CTAB fiber before and after washing with acid, 50 % ethanol and water.

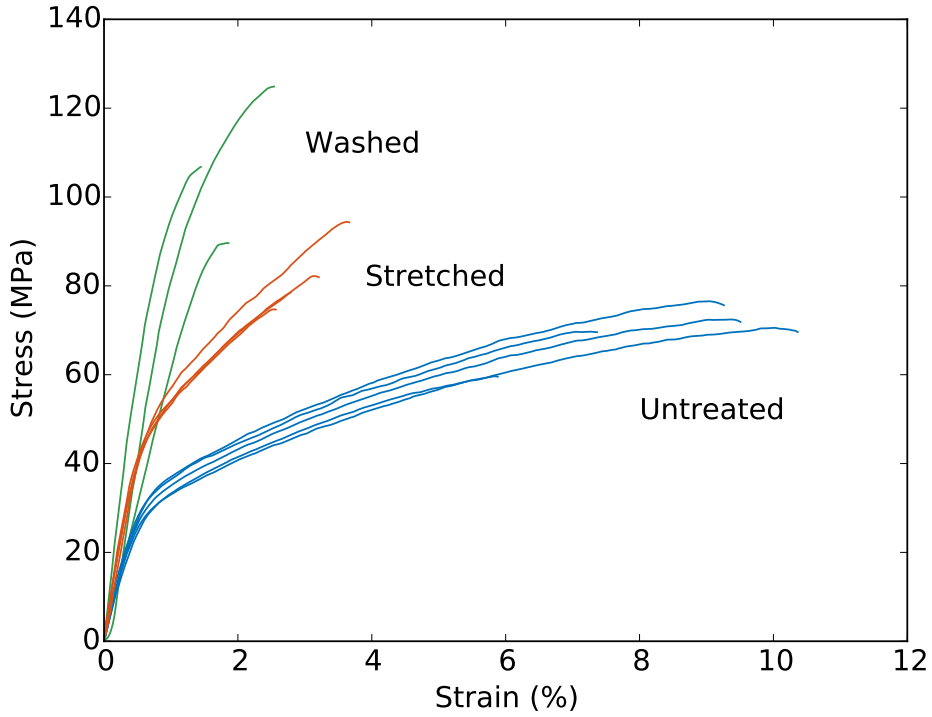

Figure 3.3: Stress-strain curves of washed, stretched and untreated TOCN-CTAB fibers.

The washed TOCN-CTAB fibers reach an average maximum strength of ca. 110 MPa, which is low compared to what is reported in the literature for CNF-based fibers and CNF reinforced nanocomposite fibers [35, 37, 39, 40]. One possible hindrance to the mechanical performance of TOCN-CTAB fibers is that CTAB adsorbed on the TOCN surfaces reduce the adhesive interaction between the CNF's. The small CTAB molecules can also diffuse deep inside the wet filament, coating all TOCN surface, thus preventing the formation of a strong hydrogen bonded network inside the fiber. The hydrophobicity of the nanofibrils would prevent them from compacting completely while drying which makes the structure prone to defects, weakening the fiber. Removal of CTAB and better compacting of the dried fiber is one likely cause to the higher ultimate tensile strength and Young's modulus of the washed TOCN-CTAB fiber, although it is still lower than similar fibers often reported in the literature [35, 37, 39, 40]. A new direction for the study was considered more viable than continuing along this path.

3.2 Cellulose nanofibril-polyelectrolyte fibers

In the second part of this work we used concepts from spinning and stretching wet TOCN-CTAB filaments and pushed them further. We sought to enhance the mechanical properties by using materials we believed would form stronger complexes, did not prevent TOCN compacting while drying, and could also be stretched more to achieve higher ultimate tensile strength and Young's modulus. The method of spinning with a linear stage was developed to counter the inconsistency of manual fiber spinning and also to achieve a constant rate of stretching. Stretchability was selected as an intermediate goal to achieve higher orientation which usually results in higher ultimate tensile strength and Young's modulus in fibers.

Cationic polymers and polysaccharides absorb on the TOCN surface well but can be chosen so that they do not make the TOCN surface hydrophobic. We selected chitosan and PDADMAC for their availability and for the reason that their interactions could be tuned with the pH and ionic strength of the solutions respectively.

3.2.1 Conditions for drawing fiber from interface

At first it was not immediately clear what kind of concentrations should be used to pull a fiber or whether or not it was possible at all. To promote the continuous flow of TOCN and polyelectrolytes to the newly forming surface it was thought that a low concentration and low viscosity would be favorable. Ranges of concentrations for which manually spinning a fiber was feasible were tested and the results are presented in tables 3.1 and 3.2.

	PDADMAC (wt. %)			
TOCN (wt. %)	20	2	0.2	0.02
0.6	no	no	no	no
0.4	**yes**	**yes**	**yes**	**yes**
0.1	no	no	**yes**	**yes**
0.05	no	no	**yes**	**yes**

Table 3.1: Concentrations of TOCN and PDADMAC with which pulling a fiber is possible

	chitosan (wt. %)		
TOCN (wt. %)	1	0.2	0.02
0.6	no	**yes**	no
0.4	**yes**	**yes**	no
0.1	**yes**	**yes**	**yes**
0.05	**yes**	**yes**	**yes**

Table 3.2: Concentrations of TOCN and chitosan with which pulling a fiber is possible

With concentrations lower than 0.1 wt. % still working well for spinning it was clear that very low concentrations could be used in this method. In contrast wet-spinning by extrusion to coagulation bath usually requires high concentrations in order for the fiber to remain intact. A TOCN concentration of 0.4 wt. % was decided to be used for later tests. This was mostly for convenience, as low concentrations resulted in extremely thin fibers which were very difficult to handle.

3.2.2 Tuning the complexation

The interactions between TOCNs and the polyelectrolytes is controlled by the number of crosslinked repeating units. This crosslinking should be hindered by reducing the number of charged repeating units in chitosan by pH changes or in the case PDADMAC, introducing NaCl to the solution which would increase the number ions that compete with bonding to TOCN fibrils. It was assumed that the fiber could be made ductile with these changes. Therefore the pH of chitosan solution and ionic strength of PDADMAC solution was assumed to affect the stretchability of the fibers.

The complexation of PDADMAC could be tuned by the ionic strength of the solution. A range of NaCl molarity of the PDADMAC solution for which it was still possible to manually spin a fiber was tested. When molarity of NaCl in 1 wt. % PDADMAC solution was above 100 mM the manual spinning failed. At 65 mM NaCl the spinning was clearly hindered, but short fibers could be drawn occasionally. At 20 mM NaCl and lower the spinning was successful. In a 1 wt. % PDADMAC solution there is ca. 60 mM of sites for ionic complexation.

The pH of chitosan solution could be used to tune the complexation of TOCN-chitosan. The pH of the solution affects the degree of deprotonation of the chitosan. A upper limit of pH for which manual

fiber spinning was feasible was attempted to be found, but chitosan started to flocculate at pH above 6.26. This prevented complexation with TOCN and rendered manual spinning infeasible. The manual spinning was successful at a pH range of 5.95-6.25.

The feasibility tests were spun manually but in order to pull as consistently as possible, the stretched fibers and mechanical testing fibers were pulled using a linear stage and a PMMA well with hydrophobic coating.

A scatter plot of the maximum stretch of wet TOCN-chitosan filaments before fracture versus the pH of chitosan solution is presented in figure 3.4. Many fibers broke at seemingly low stretch and there were some difficulties trying to achieve a reliable maximum stretch.

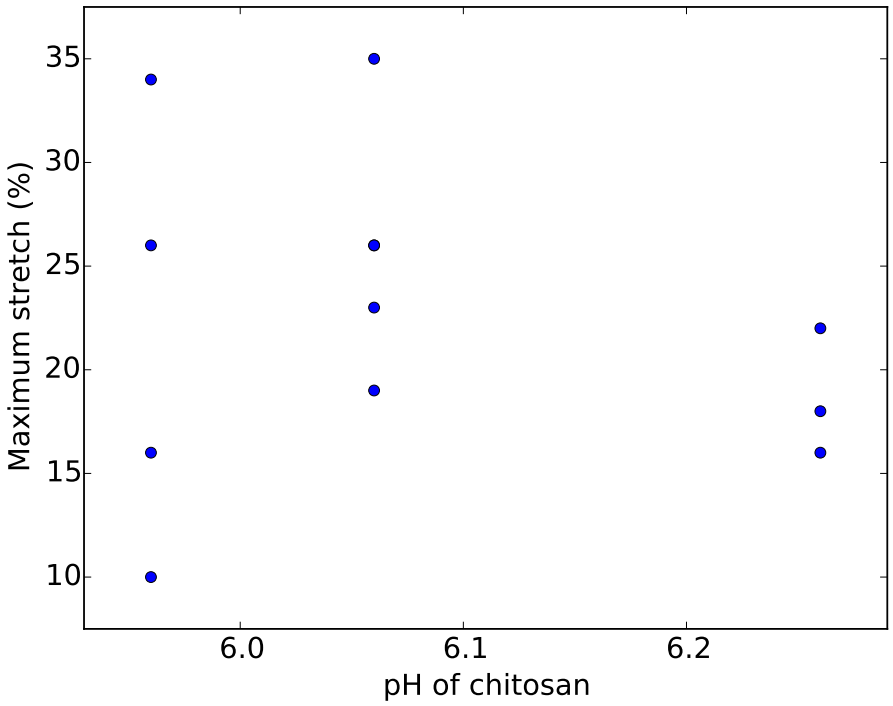

Figure 3.4: Maximum stretch of the TOCN-chitosan fiber vs. pH of chitosan solution.

A scatter plot of the maximum stretch of wet TOCN-PDADMAC filaments before fracture versus the pH of PDADMAC solution is presented in figure 3.5. The difficulties of reproducibility apparent with TOCN-chitosan fibers persisted in the case of TOCN-PDADMAC fibers.

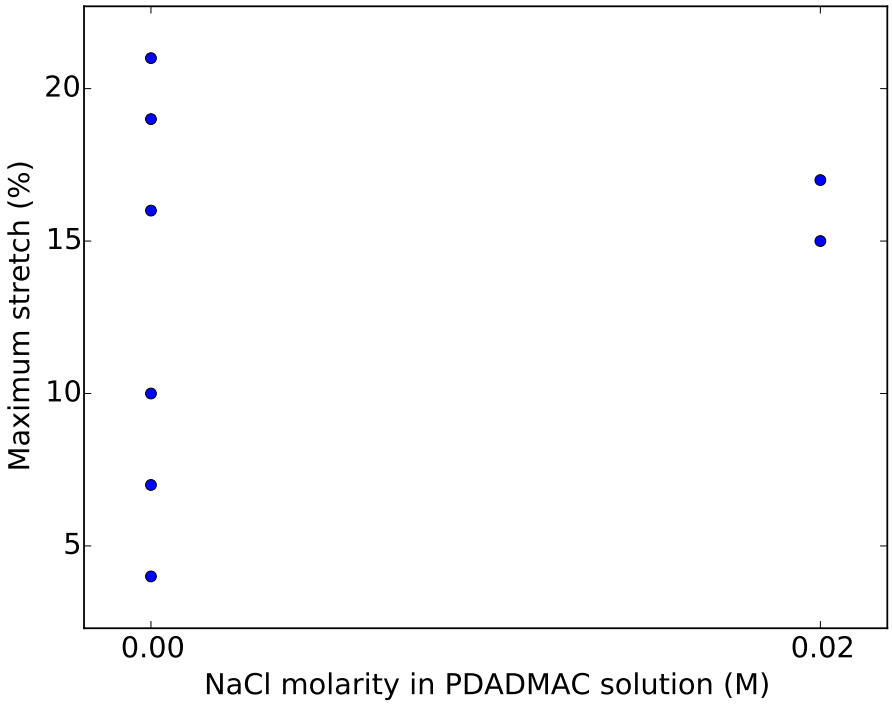

Figure 3.5: Maximum stretch of the TOCN-PDADMAC fiber vs. the ionic strength of PDADMAC solution.

A clear trend was missing in both figures 3.4 and 3.5. For following measurements 0 M NaCl molarity for PDADMAC solution and pH 5.96 for chitosan solution were chosen to be used. The reason for the inconsistencies in wet filament stretchability is unclear. The drying of the filament before stretching might have caused some hardening. Torres-Rendon et al. preformed stretching of wet-spun CNF fibers in aqueous environment preventing the drying, but also reached similar stretch ratios of 30 % [35]. It is notable that these wet filaments were strong enough to be stretched in ambient conditions to similar draw ratios than what has been achieved in an aqueous environment in the literature [35]. No orientation measurements could be performed here due to time constraints. Photos of a TOCN-polyelectrolyte filament before and after stretching are presented in figure 3.6.

A 20 % stretch causes significant improvement in tensile properties as is discussed in section 3.2.5. The achieved stretch ratios are comparable to CNF-based fibers reported in the literature [35]. Using CNF as a filler in polymer matrix results in stretch ratios much

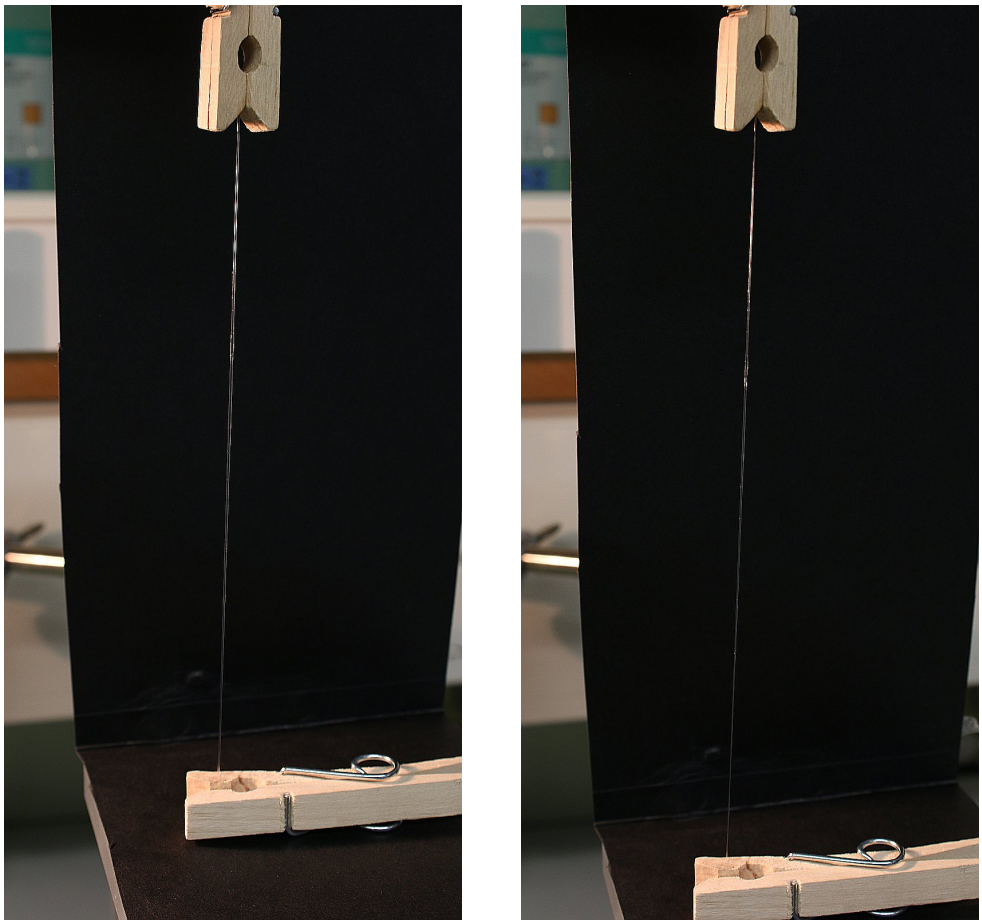

(a) Before. (b) After.

Figure 3.6: Photos of a TOCN-polyelectrolyte filament before and after stretching 20 %.

closer to those of synthetic fibers [37]. Perhaps better control of the parameters could allow for more stretch. It must be admitted that using relatively low concentrations of TOCN and polyelectrolytes in the solutions used in the pulling causes the wet filament to have a lot of excess water. The excess water causes the TOCN fibrils to have greater distance to each other and a weaker network of crosslinks. However high concentrations could not be used to pull a fiber using this method because low viscosity and good flow of TOCNs is required in the interface. A rigid network of crosslinking might also reduce the ductility of the fiber. The requirement of low viscosity might cause severe limitations to this method of spinning by interfacial complexation.

3.2.3 Cross-sectional area of the fiber

The diameter of the well had a result on the diameter of the fiber. The diameter of the fiber versus the diameter of the well is presented in figure 3.7. The diameters of the fibers were measured by optical microscope.

For well diameters 3–7 mm the fiber diameter increases linearly with the well diameter ($R^2 = 0.99$), but after that the relation is not clear anymore. The 3–7 mm range of diameters was considered as more consistent but the smallest diameter wells were difficult to handle. For this reason the 6 mm diameter well was chosen to be used.

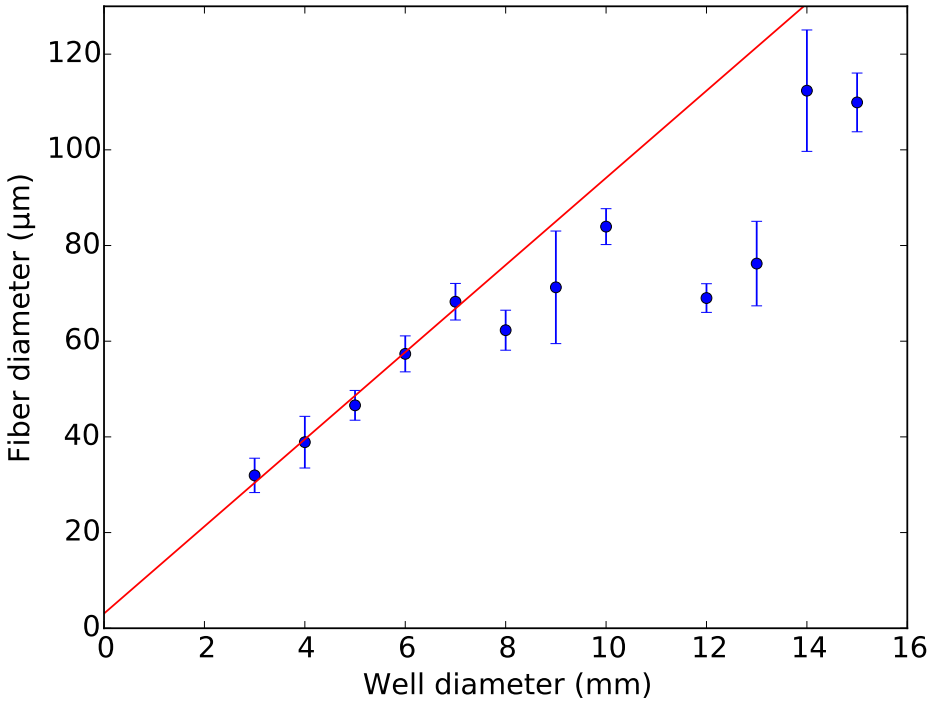

Figure 3.7: Average diameter of the fiber and its standard deviation versus the diameter of the well. The linear fit is fitted only for well diameters of 3–7 mm.

The cross-sectional area can also be measured directly after fracturing the fiber, sputtering it with Au/Pd coating and imaging the cross-section with SEM. The thickness of the metal coating is negligible. Aligning the fiber with the beam however is somewhat difficult. If the fiber is not aligned then an error is introduced to the area, roughly of the factor $1 - \sin(\theta)$, where θ is the angle between the beam and the fiber. Selected samples were imaged post-fracture with SEM and their cross-sections were measured directly with ImageJ software. The cross-sectional area was observed to be ca. 10 % smaller than what was measured by optical microscopy. This might be caused by a misaligned fiber or by dimensional changes due to plastic deformation. SEM images of the samples are further discussed in section 3.2.4.

3.2.4 Structure of the fibers

Optical microscope images from the fibers were taken to approximate the cross-sectional area of each sample. Examples of such images are presented in figure 3.8.

In some fibers Plateau-Rayleigh instability caused droplets to form on the fiber while it was drying. The droplets caused bulges in the fiber even after it was completely dry. They probably don't negatively affect the strength of the fiber because a thicker section in the fiber is assumed to be stronger than neighbouring regions. An example of a bulge in the fiber caused by Plateau-Rayleigh instability is presented in figure 3.9a. The formation of Plateau-Rayleigh instability droplets are affected by the viscosity and the rate of spinning of the fiber [45].

SEM images were taken from both stretched and unstretched TOCN-chitosan and TOCN-PDADMAC fibers. They are presented in images 3.10 and 3.11 respectively. From the SEM images we observed that the unstretched and stretched fibers are similar in microstructure. The cross-sections are also approximately circular in shape, especially the TOCN-chitosan fibers. They are also not hollow. This justifies approximating the cross-sectional area by the fiber diameter as explained in section 2.13.

Wet-spinning CNF fibers to a coagulation bath can produce porosity, hollow fibers and uncircular fibers [38–40]. The deviation from a dense morphology can deteriorate the mechanical properties of fibers but also in such cases determining the cross-sectional area of the fiber is difficult, which results in inaccuracies to the results of mechanical properties. The interfacial complexation method seems to overcome these problems.

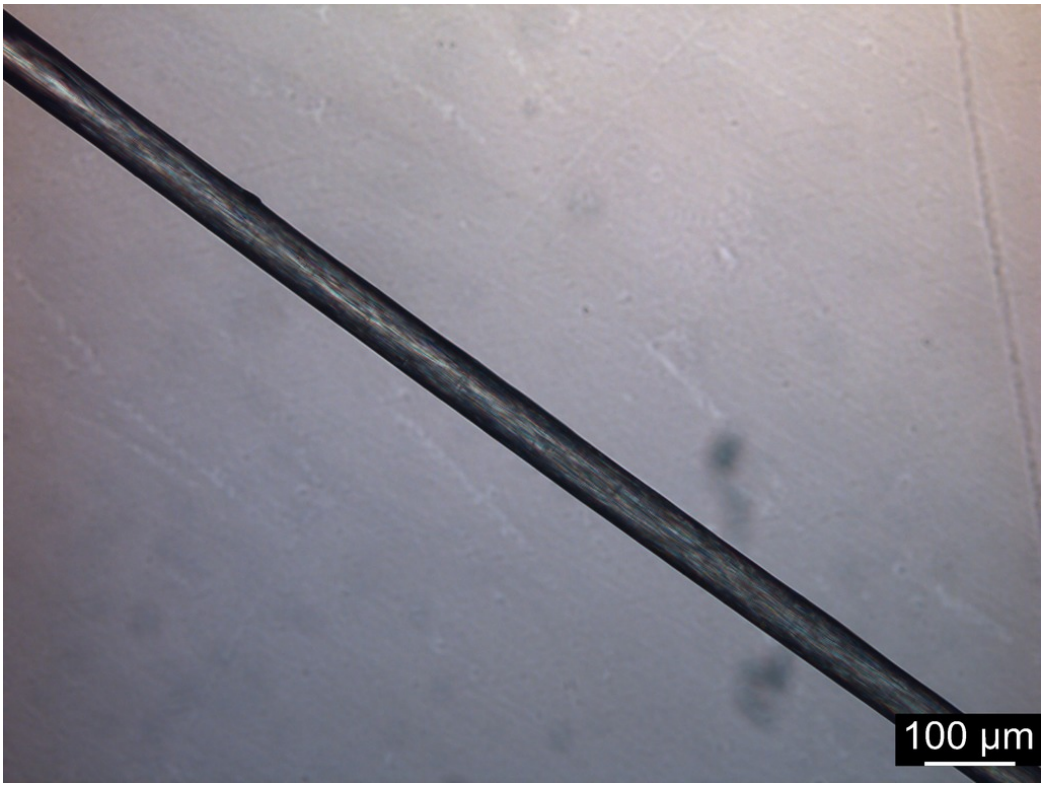

(a) TOCN-chitosan

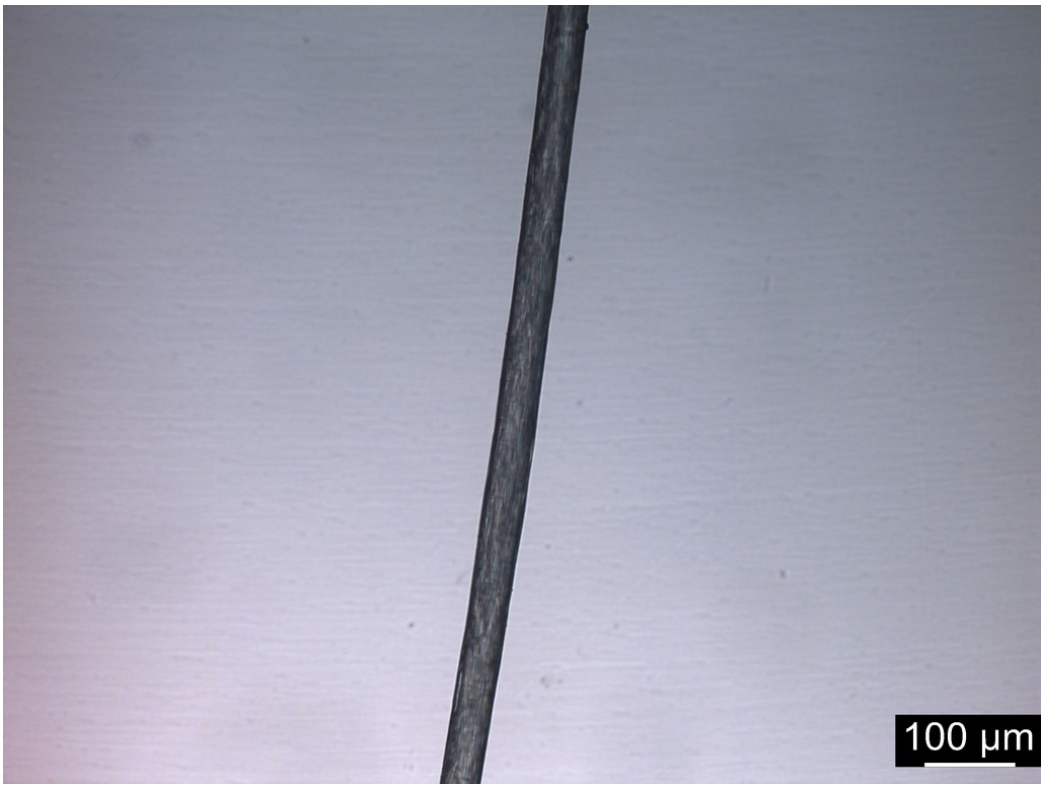

(b) TOCN-PDADMAC

Figure 3.8: Optical microscope images of TOCN-chitosan and TOCN-PDADMAC fibers.

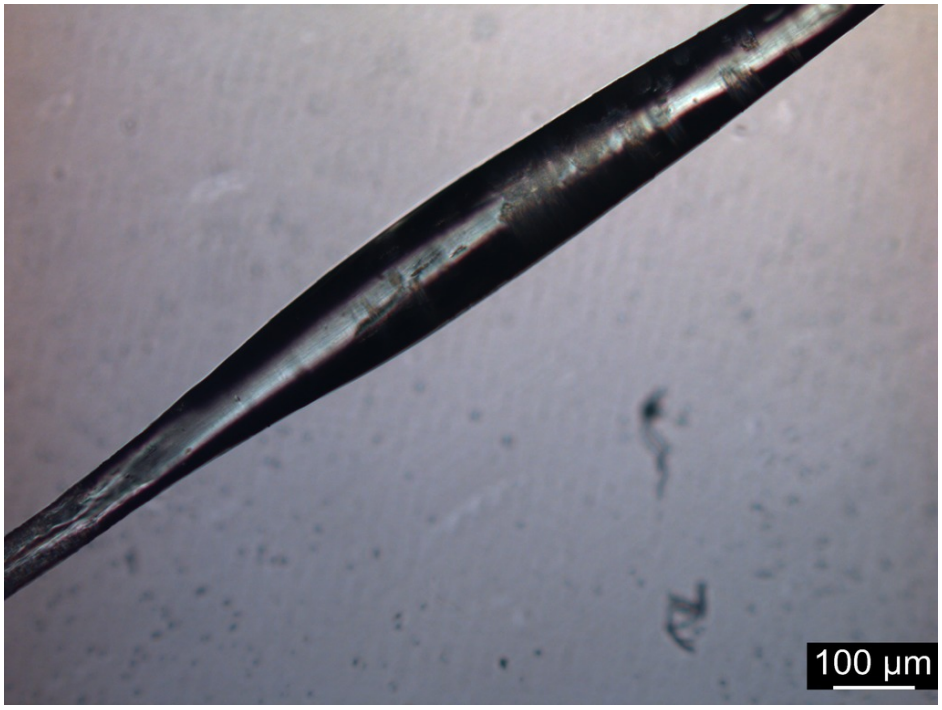

(a) A defect caused by Plateau-Rayleigh instability imaged with optical microscope.

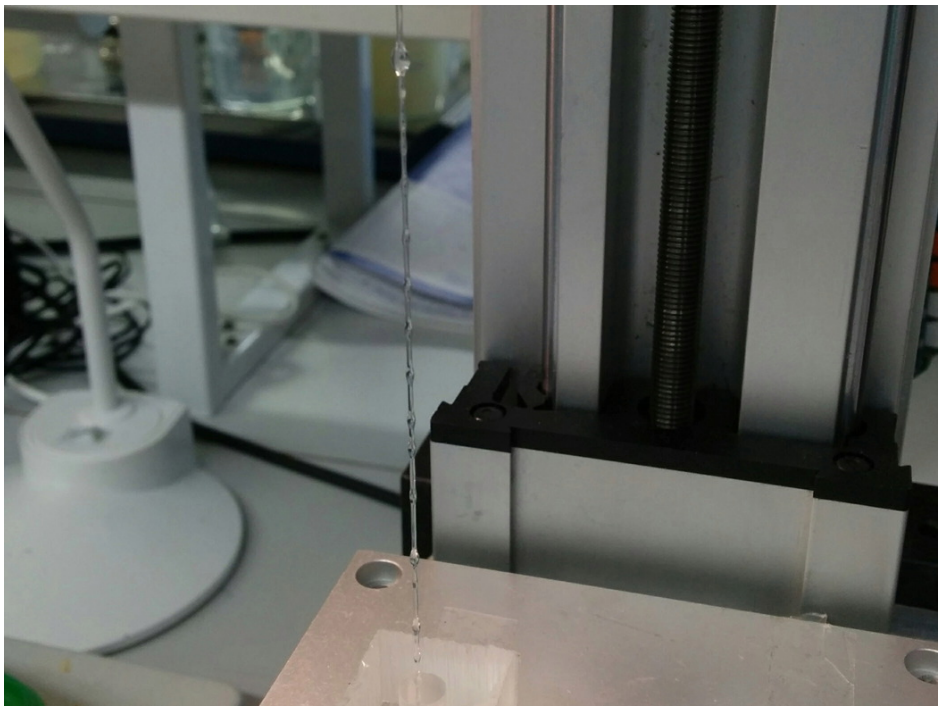

(b) A photo of a wet filament with droplets caused by Plateau-Rayleigh instability.

Figure 3.9: Observations of Plateau-Rayleigh instabilities.

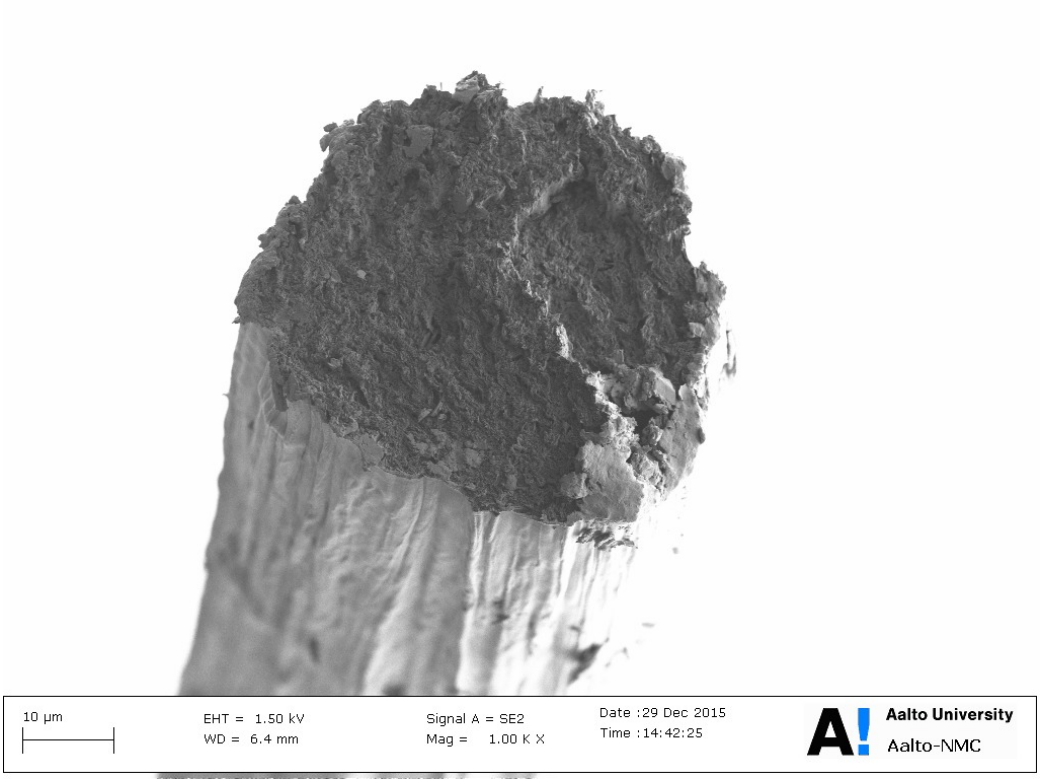

(a) Unstretched.

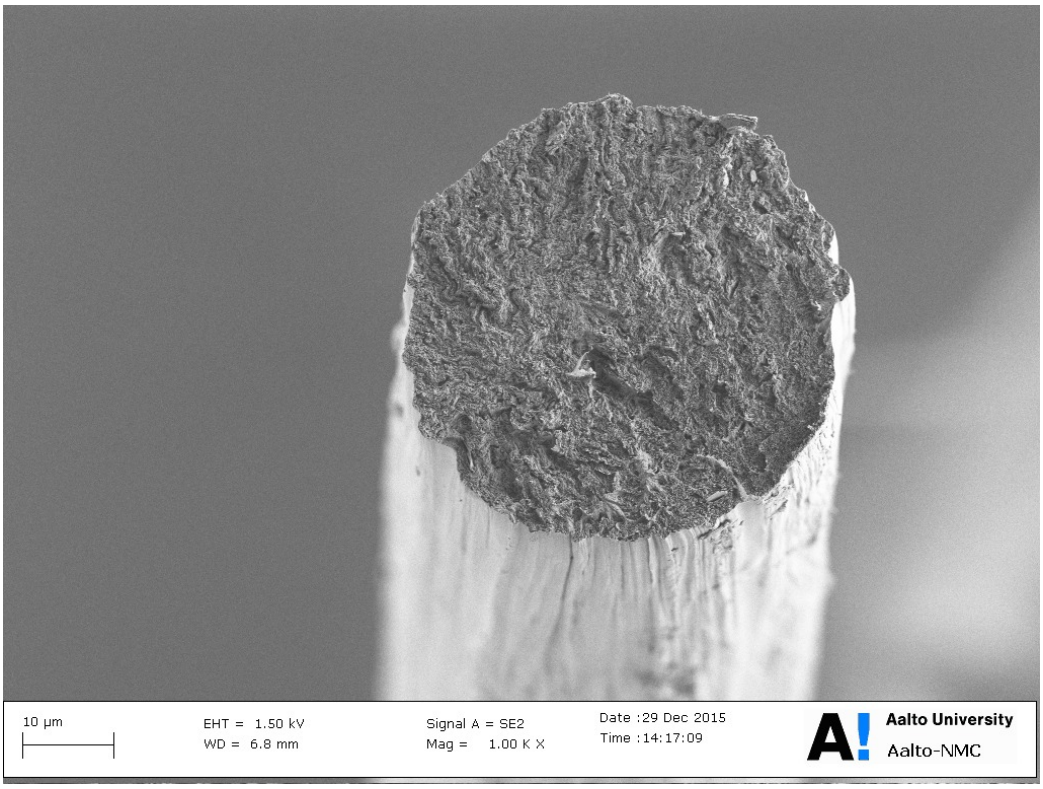

(b) Stretched 20%.

Figure 3.10: SEM of TOCN-chitosan fiber cross-sections

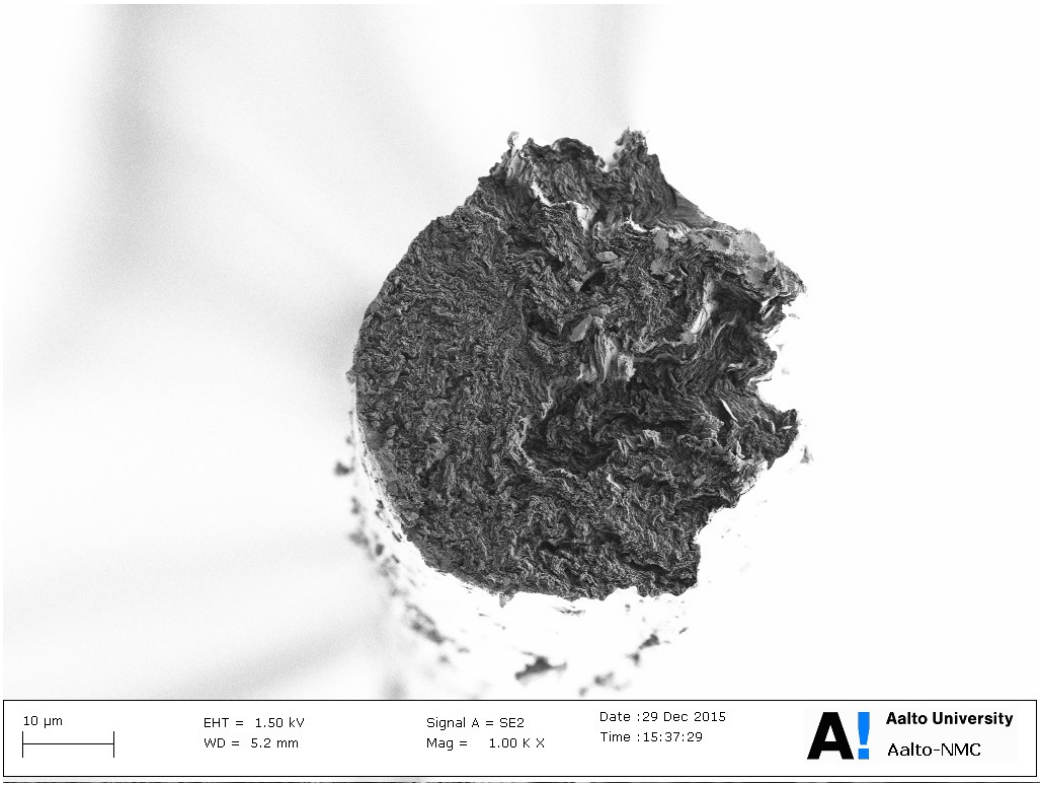

(a) Unstretched.

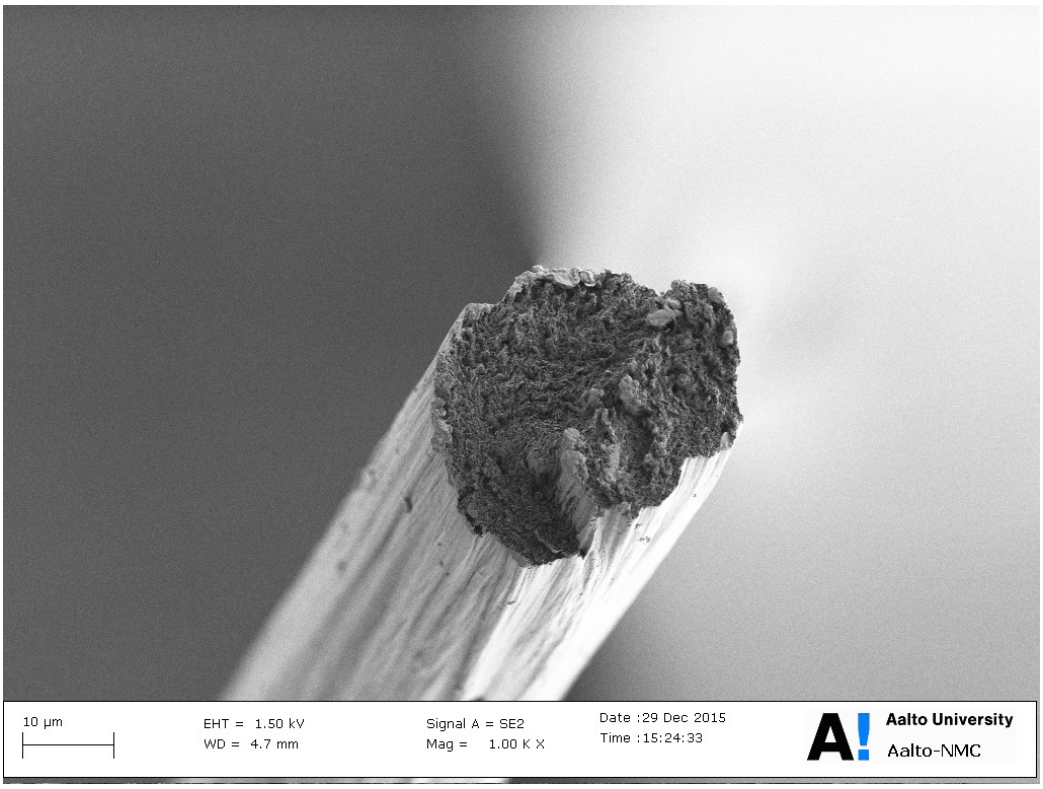

(b) Stretched 20%.

Figure 3.11: SEM of TOCN-PDADMAC fiber cross-sections.

3.2.5 Tensile properties

Stress-strain curves of the TOCN-polyelectrolyte fibers are presented in figure 3.12. The relative humidity during tensile testing was 43–53 % at 22–23 °C. Results of all mechanical testing performed in this work are summarized in table 3.3 and compared to other results reported in the literature.

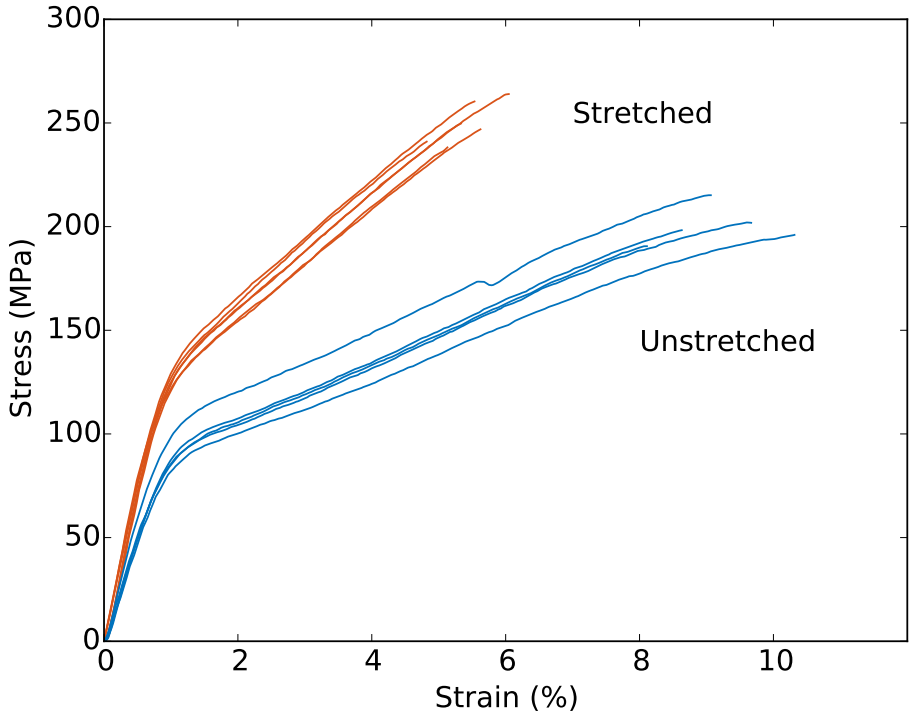

(a) TOCN-chitosan

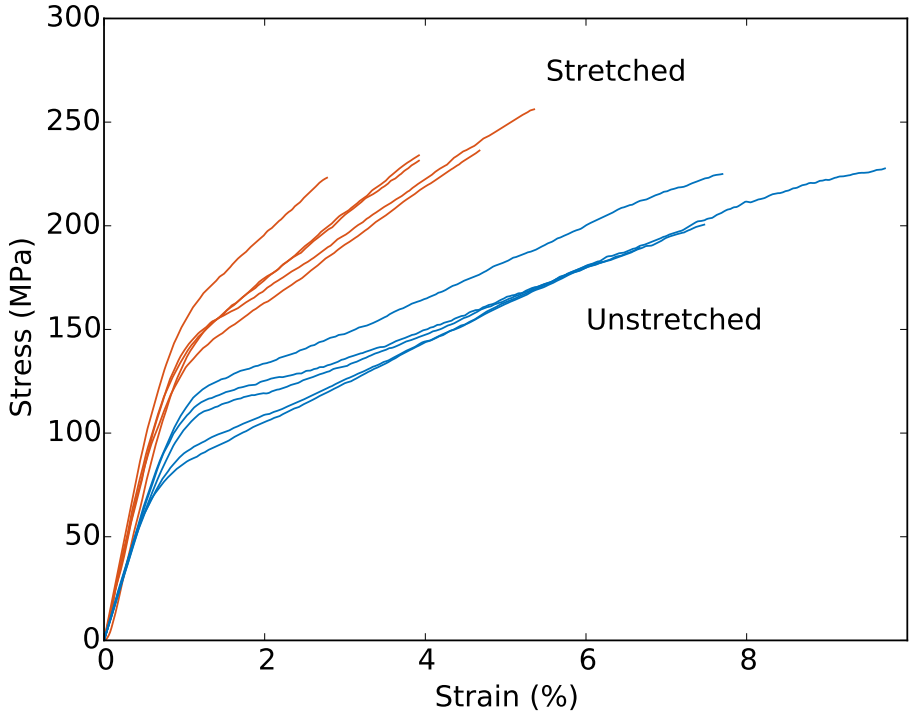

(b) TOCN-PDADMAC

Figure 3.12: Stress-strain curves of TOCN-polyelectrolyte fibers.

	Material	Form	S (%)	σ_U (MPa)	ε_U (%)	YM (GPa)
This work						
chitosan-0%	TOCN	Fiber	0	200±9	9.2±0.9	15±1
chitosan-20%	TOCN	Fiber	20	250±10	5.4±0.4	20±2
PDADMAC-0%	TOCN	Fiber	0	205±21	7.6±1.4	15±1
PDADMAC-20%	TOCN	Fiber	20	236±12	4.1±1.0	23±5
CTAB-washed	TOCN	Fiber	0	107±18	1.9±0.6	13±4
CTAB-20%	TOCN	Fiber	20	82±9	3.1±0.5	12±1
CTAB-0%	TOCN	Fiber	0	70±6	8.5±1.8	10±3
Literature						
Iwamoto et al. [38]	TOCN	Fiber	0	321±145	2.2±1.2	24±2
Walther et al. [34]	TOCN	Fiber	0	275±15	4.0±0.2	23±0.4
Torres-Rendon et al. [35]	TOCN	Fiber	28	289±37	1.6±0.3	34±4
Håkansson et al. [41]	CMCNF	Fiber	0	490±86	6.4±1.6	18±1
Hooshmand et al. [39]	CNF	Fiber	0	222±16	∼3±-	13±2
Sehaqui et al. [53]	TOCN	Film	60	397±-	1.8±-	33±-
Henriksson et al. [54]	CNF	Film	0	214±7	10.1±1.4	5±13
Galland et al. [55]	CNF	Film	0	319±9	7.1±0.4	16±1

Table 3.3: Summary of mechanical properties of the fibers presented in this work and those of relevant CNF-based fibers and films presented in the literature. Some values are missing from the publications (marked -) and some values are estimated from the stress-strain curves in the publications (marked $\sim$). S denotes stretching before tensile testing, σ_U denotes ultimate tensile strength, ε_U denotes ultimate tensile strain and YM denotes Young's modulus.

The ultimate tensile strengths and Young's moduli of the TOCN-polyelectrolyte fibers are comparable to other CNF-based fibers reported in the literature [34, 35, 38, 39].

The stretching of the fibers resulted in significant improvement in the Young's modulus, the ultimate tensile strength and the yield strength, but a reduction in the ultimate tensile strain for both TOCN-chitosan and TOCN-PDADMAC fibers. This is commonly observed in fibers and CNF nanocomposites [35, 40]. In TOCN-chitosan fibers the tensile strength improved by 25 % from 200 to 250 MPa and Young's modulus improved by 33 % from 15 to 20 GPa by a mere 20 % stretch. In TOCN-PDADMAC fibers the improvements were similar, tensile strength improved by 15 % from 205 to 236 MPa and Young's modulus improved by 53 % from 15 to 23 GPa.

In 2014 Torres-Rendon et al. achieved similar improvements in strength by preparing CNF fibers by extrusion into a coagulation bath followed by drying. Subsequently the dry fibers were immersed water and stretched up to 30 % while submerged [35]. The tensile strength of the fiber improved by 60 % from 118 to 189 MPa. The improvements in Young's modulus were proportionally much larger, 410 % from 8.2 to 33.7 GPa. The fiber has the highest Young's modulus in table 3.3, and also the lowest tensile strain. The unstretched fibers in the Torres-Rendon et al. publication have an ultimate tensile strain of 8.3 %, comparable to the unstretched fibers in this work. This suggests that the fibers prepared in this work by interfacial complexation may have potential for even further prestretching in the wet state as their ultimate tensile strain did not decrease as dramatically as in the work by Torres-Rendon et al. [35].

In 2012 Sehaqui et al. prepared TOCN films of high strength and stiffness by vacuum filtration of TOCN dispersion [53]. The wet films could be Stretched up to 60 % by having them dry partially until water content was 70–90 wt. %. The films were then dried. The orientation indices of the stretched film were high, 82 % in plane and 89 % cross-sectionally. Stretching also resulted in significant improvements in mechanical properties: Strength improved from 185 MPa to 400 MPa and Young's modulus improved from 10 GPa to 33 GPa [53]. It should be noted that the stretching was performed in high TOCN concentrations of 10–30 wt. %. Perhaps with the right stretching conditions filaments prepared by interfacial complexation similar to this work could also be stretched to higher ratios.

In 2014 Håkansson et al. prepared CNF-based fibers with a very high strength of 490 MPa using microfluidic flow focusing [40]. The

shear forces caused by accelerating a jet of CNF suspension induces alignment of the nanofibrils and subsequent gelation locks the oriented nanofibrils in place. This causes orientation of the fiber without an additional process of stretching after spinning. Håkansson et al. also used carboxymethylated CNF (CMCNF) prepared in the exact same way as in a study conducted in 2008 by Henriksson et al. for better comparison, even though the latter studied CNF in the form of a film instead of a fiber [40, 54]. The strengths of the films achieved by Henriksson et al. were similar to many other CNF-based films, 214 MPa, so the extraordinary strength of the fiber achieved by Håkansson et al. can not be attributed to variations in the CNF raw material [54].

In 2014 Peng et al. prepared PVA-CNF composite fibers and achieved a tensile strength of 828 MPa and a Young's modulus of 32 GPa [37]. They used at maximum 6 wt. % of CNF as a filler material inside the PVA matrix which allowed them to stretch the fiber up to 2700 % causing also very high orientation indices above 95 % Because of the low CNF content this fiber is not comparable to fibers consisting mostly of CNF, although it has a very high strength and is stronger than either PVA or CNF fibers by themselves [37]. This suggests that a very high orientation of the nanofibrils increases the strength and stiffness of the fibers significantly. Stretching CNF fibers to a high stretch ratio is difficult however, as observed in this work and by Torres-Rendon et al [35].

Maybe by simply a careful selection of the interfacial complexation and stretching conditions and the polyelectrolyte one could achieve higher stretch ratios. Perhaps if one could prepare a highly elastic interfacial complex containing TOCN and stretch it to align the nanofibrils one might achieve highly oriented TOCN fibers. Stretching the fibers while submerged in water could also facilitate stretching with lower speeds, as in ambient conditions the fibers eventually dry out, reducing CNF and polyelectrolyte mobility.

Chapter 4

Conclusions

We successfully spun CNF-based continuous macrofibers by interfacial complexation and reached tensile strengths up to 250 MPa. The interfacial complexation could be preformed with anionic TOCNs and three different types of cationic moieties: cationic surfactant CTAB, polycation PDADMAC and cationic polysaccharide chitosan. The supramolecular interactions of TOCN-PDADMAC could be tuned with ionic strength. The tuning of ionic interactions of TOCN-chitosan by pH was attempted. All three types of fibers could be stretched 20 % before drying which resulted in enhanced tensile strength, yield strength and Young's modulus, but decreased ultimate tensile strain. The mechanical properties of the fibers are similar to many other CNF-based macrofibers reported in the literature as presented in table 3.3 [34, 35, 38–40]. Orientation indices and order parameters were not measured. The TOCN-CTAB fibers could be post-treated with acid, ethanol and water solutions to remove CTAB and enhance the mechanical strength and Young's modulus.

Methods for reliable measurement of the fiber diameter were compared critically. The error of the fiber diameter greatly increases the error in cross-sectional area and mechanical strength due to quadratic scaling. The commonly used micrometer screw was dismissed as wildly inaccurate for fibers with diameter of less than 100 µm. Optical microscopy and accompanied measuring software was deemed accurate enough for circular, non-hollow and low-porosity fibers.

The microstructure of the fibers was observed using SEM. The fibers were compact, non-porous and had circular cross section. Some fibers had visible bulges resulting from the Plateau-Rayleigh instability during the drying. Fibers could be spun manually but a computer controlled linear stage built for spinning was much more stable and

consistent. The diameter of the fiber could be controlled with the spinning setup.

This was the first time, to the authors knowledge, that CNF-based fibers were spun using interfacial complexation. The fibers were relatively strong compared to many similar fibers reported in the literature, but enhancing the strength and Young's modulus of CNF fibers remains as a strong future research interest. CNF fibers could have potential applications in e.g. nanocomposites, textiles, structural materials and biomedical engineering [34, 35, 39].

In the future the orientation indices could be measured for more quantitative information about the results of stretching. The method of interfacial complexation could perhaps be improved by optimising the spinning parameters, such as polyelectrolyte molecular weight and solution concentration, to achieve greater stretching and alignment. Also the stretching could be facilitated by performing it in aqueous conditions.

Bibliography

(1) Moon, R. J.; Martini, A.; Nairn, J.; Simonsen, J.; Youngblood, J. *Chemical Society Reviews* **2011**, *40*, 3941–3994.

(2) Sehaqui, H.; Zimmermann, T.; Tingaut, P. *Cellulose* **2013**, *21*, 367–382.

(3) Klemm, D.; Heublein, B.; Fink, H.-P.; Bohn, A. *Angewandte Chemie International Edition* **2005**, *44*, 3358–3393.

(4) Eichhorn, S. J.; Dufresne, A.; Aranguren, M.; Marcovich, N. E.; Capadona, J. R.; Rowan, S. J.; Weder, C.; Thielemans, W.; Roman, M.; Renneckar, S.; Gindl, W.; Veigel, S.; Keckes, J.; Yano, H.; Abe, K.; Nogi, M.; Nakagaito, A. N.; Mangalam, A.; Simonsen, J.; Benight, A. S.; Bismarck, A.; Berglund, L. A.; Peijs, T. *Journal of Materials Science* **2009**, *45*, 1–33.

(5) Postek, M. T.; Vladár, A.; Dagata, J.; Farkas, N.; Ming, B.; Wagner, R.; Raman, A.; Moon, R. J.; Sabo, R.; Wegner, T. H.; Beecher, J. *Measurement Science and Technology* **2011**, *22*, 024005.

(6) Myllytie, P. *Interactions of polymers with fibrillar structure of cellulose fibers: A new approach to bonding and strength in paper*, Doctoral thesis, Aalto University, **2009**.

(7) Kettunen née Pääkkö, M. *Cellulose Nanofibrils as a Functional Material*, Doctoral thesis, Aalto University, **2013**.

(8) Klemm, D.; Kramer, F.; Moritz, S.; Lindström, T.; Ankerfors, M.; Gray, D.; Dorris, A. *Angewandte Chemie International Edition* **2011**, *50*, 5438–5466.

(9) Brongniart, A.; Guillemin, A.; Decaisne, J.; Van Tieghem, P.; Costantin, J.; Allorge, P.; Blaringhem, L., *Annales des sciences naturelles: Botanique et biologie végétale*; Masson: **1839**, pp 21–31.

(10) Eichhorn, S.; Davies, G. *Cellulose* **2006**, *13*, 291–307.

(11) Diddens, I.; Murphy, B.; Krisch, M.; Müller, M. *Macromolecules* **2008**, *41*, 9755–9759.

(12) Nishiyama, Y.; Sugiyama, J.; Chanzy, H.; Langan, P. *Journal of the American Chemical Society* **2003**, *125*, 14300–14306.

(13) Habibi, Y.; Lucia, L. A.; Rojas, O. J. *Chemical Reviews* **2010**, *110*, 3479–3500.

(14) Fernandes, A. N.; Thomas, L. H.; Altaner, C. M.; Callow, P.; Forsyth, V. T.; Apperley, D. C.; Kennedy, C. J.; Jarvis, M. C. *Proceedings of the National Academy of Sciences* **2011**, *108*, E1195–E1203.

(15) Somerville, C.; Bauer, S.; Brininstool, G.; Facette, M.; Hamann, T.; Milne, J.; Osborne, E.; Paredez, A.; Persson, S.; Raab, T.; Vorwerk, S.; Youngs, H. *Science* **2004**, *306*, 2206–2211.

(16) Nishiyama, Y. *Journal of Wood Science* **2009**, *55*, 241–249.

(17) Lee, K.-Y.; Aitomäki, Y.; Berglund, L. A.; Oksman, K.; Bismarck, A. *Composites Science and Technology* **2014**, *105*, 15–27.

(18) Khalil, H. P. S. A.; Davoudpour, Y.; Islam, M. N.; Mustapha, A.; Sudesh, K.; Dungani, R.; Jawaid, M. *Carbohydrate Polymers* **2014**, *99*, 649 –665.

(19) Svagan, A. J.; Azizi Samir, M. A. S.; Berglund, L. A. *Biomacromolecules* **2007**, *8*, 2556–2563.

(20) Yano, H.; Sugiyama, J.; Nakagaito, A. N.; Nogi, M.; Matsuura, T.; Hikita, M.; Handa, K. *Advanced Materials* **2005**, *17*, 153–155.

(21) Nogi, M.; Iwamoto, S.; Nakagaito, A. N.; Yano, H. *Advanced Materials* **2009**, *21*, 1595–1598.

(22) Klemm, D.; Schumann, D.; Kramer, F.; Heßler, N.; Koth, D.; Sultanova, B. *Macromolecular Symposia* **2009**, *280*, 60–71.

(23) Pääkkö, M.; Vapaavuori, J.; Silvennoinen, R.; Kosonen, H.; Ankerfors, M.; Lindström, T.; Berglund, L. A.; Ikkala, O. *Soft Matter* **2008**, *4*, 2492–2499.

(24) Pääkkö, M.; Ankerfors, M.; Kosonen, H.; Nykänen, A.; Ahola, S.; Österberg, M.; Ruokolainen, J.; Laine, J.; Larsson, P. T.; Ikkala, O.; Lindström, T. *Biomacromolecules* **2007**, *8*, 1934–1941.

(25) Siró, I.; Plackett, D. *Cellulose* **2010**, *17*, 459–494.

(26) Usov, I.; Mezzenga, R. *Macromolecules* **2015**, *48*, 1269–1280.

(27) Arola, S.; Malho, J.; Laaksonen, P.; Lille, M.; Linder, M. B. *Soft Matter* **2013**, *9*, 1319–1326.

(28) Nogi, M.; Handa, K.; Nakagaito, A. N.; Yano, H. *Applied Physics Letters* **2005**, *87* 243110.

(29) Nogi, M.; Ifuku, S.; Abe, K.; Handa, K.; Nakagaito, A. N.; Yano, H. *Applied Physics Letters* **2006**, *88* 133124.

(30) Juntaro, J.; Pommet, M.; Kalinka, G.; Mantalaris, A.; Shaffer, M. S. P.; Bismarck, A. *Advanced Materials* **2008**, *20*, 3122–3126.

(31) Saito, T.; Nishiyama, Y.; Putaux, J.-L.; Vignon, M.; Isogai, A. *Biomacromolecules* **2006**, *7*, 1687–1691.

(32) Isogai, A.; Kato, Y. *Cellulose* **1998**, *5*, 153–164.

(33) Isogai, A.; Saito, T.; Fukuzumi, H. *Nanoscale* **2011**, *3*, 71–85.

(34) Walther, A.; Timonen, J. V. I.; Díez, I.; Laukkanen, A.; Ikkala, O. *Advanced Materials* **2011**, *23*, 2924–2928.

(35) Torres-Rendon, J. G.; Schacher, F. H.; Ifuku, S.; Walther, A. *Biomacromolecules* **2014**, *15*, 2709–2717.

(36) Nishino, T.; Takano, K.; Nakamae, K. *Journal of Polymer Science Part B: Polymer Physics* **1995**, *33*, 1647–1651.

(37) Peng, J.; Ellingham, T.; Sabo, R.; Turng, L.-S.; Clemons, C. M. *Cellulose* **2014**, *21*, 4287–4298.

(38) Iwamoto, S.; Isogai, A.; Iwata, T. *Biomacromolecules* **2011**, *12*, 831–836.

(39) Hooshmand, S.; Aitomäki, Y.; Norberg, N.; Mathew, A. P.; Oksman, K. *ACS Applied Materials & Interfaces* **2015**, *7*, 13022–13028.

(40) Håkansson, K. M. O.; Fall, A. B.; Lundell, F.; Yu, S.; Krywka, C.; Roth, S. V.; Santoro, G.; Kvick, M.; Prahl Wittberg, L.; Wågberg, L.; Söderberg, L. D. *Nature Communications* **2014**, *5*.

(41) Håkansson, K. M. O. *RSC Advances* **2015**, *5*, 18601–18608.

(42) Schaaf, P.; Schlenoff, J. B. *Advanced Materials* **2015**, *27*, 2420–2432.

(43) Hariri, H. H.; Schlenoff, J. B. *Macromolecules* **2010**, *43*, 8656–8663.

(44) Porcel, C. H.; Schlenoff, J. B. *Biomacromolecules* **2009**, *10*, 2968–2975.

(45) Wan, A. C.; Cutiongco, M. F.; Tai, B. C.; Leong, M. F.; Lu, H. F.; Yim, E. K. *Materials Today* **2016**, in press.

(46) Luo, F.; Sun, T. L.; Nakajima, T.; Kurokawa, T.; Zhao, Y.; Sato, K.; Ihsan, A. B.; Li, X.; Guo, H.; Gong, J. P. *Advanced Materials* **2015**, *27*, 2722–2727.

(47) Wan, A. C. A.; Liao, I.-C.; Yim, E. K. F.; Leong, K. W. *Macromolecules* **2004**, *37*, 7019–7025.

(48) Ohkawa, K.; Takahashi, Y.; Yamada, M.; Yamamoto, H. *Macromolecular Materials and Engineering* **2001**, *286*, 168–175.

(49) Hachisu, M.; Ohkawa, K.; Yamamoto, H. *Macromolecular Bioscience* **2003**, *3*, 92–99.

(50) Tian, Y.; Zhu, C.; Gong, J.; Ma, J.; Xu, J. *European Polymer Journal* **2015**, *73*, 127–136.

(51) Baker, A. M. E; Windle, A. H *Polymer* **2001**, *42*, 651–665.

(52) Tang, H.; Butchosa, N.; Zhou, Q. *Advanced Materials* **2015**, *27*, 2070–2076.

(53) Sehaqui, H.; Ezekiel Mushi, N.; Morimune, S.; Salajkova, M.; Nishino, T.; Berglund, L. A. *ACS Applied Materials & Interfaces* **2012**, *4*, 1043–1049.

(54) Henriksson, M.; Berglund, L. A.; Isaksson, P.; Lindström, T.; Nishino, T. *Biomacromolecules* **2008**, *9*, 1579–1585.

(55) Galland, S.; Berthold, F.; Prakobna, K.; Berglund, L. A. *Biomacromolecules* **2015**, *16*, 2427–2435.